TITLE: Age-associated contraction of tumor-specific T cells impairs antitumor immunity

Authors: Peter Georgiev[#1,2,3], SeongJun Han[#1,2,3], Amy Y. Huang[1,3,4], Thao H. Nguyen[1,3], Jefte M. Drijvers[1,2,3], Hannah Creasey[1,3], Joseph A. Pereira[1,3], Cong-Hui Yao[2,3], Joon Seok Park[1,3], Thomas S. Conway[1,3], Megan E. Fung[1,3], Dan Liang[1,3], Michael Peluso[1,3], Shakchhi Joshi[2,3], Jared H. Rowe[1,2,3,5], Brian C. Miller[6,7,8,9], Gordon J. Freeman[10], Arlene H. Sharpe[*1,3] Marcia C. Haigis[*2,3], and Alison E. Ringel[*11,12,13]

1. Department of Immunology, Blavatnik Institute, Harvard Medical School, Boston, Massachusetts 02115, USA.
2. Department of Cell Biology, Blavatnik Institute, Harvard Medical School, Boston, Massachusetts 02115, USA.
3. Gene Lay Institute of Immunology and Inflammation of Brigham and Women's Hospital, Massachusetts General Hospital and Harvard Medical School, Boston, Massachusetts 02115, USA.
4. Division of Population Sciences, Dana-Farber Cancer Institute, Boston, Massachusetts 02115, USA.
5. Department of Pediatric Oncology, Dana-Farber Cancer Institute, Boston, Massachusetts 02215, USA.
6. Department of Medicine, Division of Oncology, University of North Carolina at Chapel Hill, Chapel Hill, North Carolina 27599, USA.
7. Department of Genetics, University of North Carolina at Chapel Hill, Chapel Hill, North Carolina 27599, USA.
8. Department of Microbiology and Immunology, University of North Carolina at Chapel Hill, Chapel Hill, North Carolina 27599, USA.
9. Lineberger Comprehensive Cancer Center, University of North Carolina at Chapel Hill, Chapel Hill, North Carolina 27599, USA.
10. Department of Medical Oncology, Dana-Farber Cancer Institute and Harvard Medical School, Boston, MA, 02215, USA.
11. Ragon Institute of Mass General, MIT, and Harvard, Cambridge, Massachusetts 02139, USA.
12. Department of Biology, Massachusetts Institute of Technology, Cambridge, Massachusetts 02139, USA.
13. David H. Koch Institute for Integrative Cancer Research, Massachusetts Institute of Technology, Cambridge, Massachusetts 02142, USA.

#Contributed equally

***Co-corresponding authors**: Alison E. Ringel, Ragon Institute, 600 Main Street, Cambridge, MA 02139. E-mail: aringel@mit.edu; Arlene H. Sharpe, Harvard Medical School, New Research Building 0837, 77 Avenue Louis Pasteur, Boston, MA 02215. E-mail: arlene_sharpe@hms.harvard.edu; and Marcia C. Haigis, LHRRB Room 301A, 240 Longwood Avenue, Boston, MA 02115. E-mail: marcia_haigis@hms.harvard.edu

Running Title: Age-associated T-cell deficits impair antitumor immunity

Keywords: Antitumor immunity, Aging, $CD8^+$ T cells, Immune checkpoint blockade

Conflicts of Interest Disclosure: S.H. has consulted for Merck KGaA. P.G. has consulted for RA Capital and Astro Therapeutics. A.H.S. currently has funding from AbbVie, Taiwan Bio, and Calico unrelated to the submitted work. A.H.S. serves on advisory boards for Elpiscience, Monopteros, Fibrogen, IOME, Alixia, Corner Therapeutics, Bioentre, Glaxo Smith Kline, Amgen, and Janssen. She also is on scientific advisory boards for the Massachusetts General Cancer Center, Program in Cellular and Molecular Medicine at Boston Children's Hospital, the Human Oncology and Pathogenesis Program at Memorial Sloan Kettering Cancer Center, Perlmutter Cancer Center at NYU, the Gladstone Institutes and the Johns Hopkins Bloomberg-Kimmel Institute for Cancer Immunotherapy. She is an academic editor for the Journal of Experimental Medicine. A.H.S. has patents/pending royalties on the PD-1 pathway from Roche and Novartis. M.C.H. has patents pending on the PHD3 pathway, is on the scientific advisory board for Minovia, Alixia, and MitoQ. G.J.F. has patents/pending royalties on the PD-L1/PD-1 pathway from Bristol-Myers-Squibb, Roche, Eli Lilly, and Novartis. G.J.F. has served on advisory boards for iTeos, NextPoint, IgM, GV20, IOME, Bioentre, Santa Ana Bio, Simcere of America, and Geode. G.J.F. has equity in Nextpoint, Triursus, Xios, iTeos, IgM, Trillium, Invaria, GV20, Bioentre, and Geode. B.C.M. has consulted for Rheos Medicines, Cellarity, LifeOmic, and Telix Pharmaceuticals

Funding information: This work was supported by NIH P01 AI056299, P50 CA101942, and P01 CA236749 (to G.J.F and A.H.S.), NIH U54 CA224088, and R01CA276866 (to A.H.S. and M.C.H.), and the Ludwig Center at Harvard Medical School, NIH U01 CA267827, and the Paul F. Glenn Foundation for Medical Research to M.C.H. S.H. was supported by the Banting postdoctoral fellowship from the Canadian Institutes of Health Research (CIHR), P.G. was supported by a predoctoral NIH fellowship 1F31CA281090-01, and J.D. was supported by a predoctoral NIH fellowship 5F31CA224601. J.S.P. was supported by NIH/NCI F32-CA247072. B.C.M. is supported by the Burroughs Wellcome Fund Career Award for Medical Scientists and NIH K08CA248960. A.E.R. was supported by NIH K22 CA266150, as well as postdoctoral fellowships from the American Cancer Society (130373-PF-17-132-01-CCG) and Cell Biology Education and Fellowship Fund at Harvard Medical School.

ABSTRACT

Progressive decline of the adaptive immune system with increasing age coincides with a sharp increase in cancer incidence. In this study, we set out to understand whether deficits in antitumor immunity with advanced age promote tumor progression and/or drive resistance to immunotherapy. We found that multiple syngeneic cancers grew more rapidly in aged versus young adult mice, driven by dysfunctional $CD8^+$ T-cell responses. By systematically mapping immune cell profiles within tumors, we identified loss of tumor antigen–specific $CD8^+$ T cells as a primary feature accelerating the growth of tumors in aged mice and driving resistance to immunotherapy. When antigen-specific T cells from young adult mice were administered to aged mice, tumor outgrowth was delayed and the aged animals became sensitive to PD-1 blockade. These studies reveal how age-associated $CD8^+$ T-cell dysfunction may license tumorigenesis in elderly patients and have important implications for the use of aged mice as pre-clinical models of aging and cancer.

SYNOPSIS

Immune function declines with age. The authors show that loss of tumor antigen–specific $CD8^+$ T cells drives tumor growth and resistance to anti–PD-1 immunotherapy in aged mice, providing insight for designing immunotherapies for elderly patients.

INTRODUCTION

Aging is a complex physiological process, involving molecular, cellular, and systemic changes that increase susceptibility to disease and diminish resilience under stress (1,2). Alterations in the immune system are an established hallmark of aging, contributing to chronic low-grade inflammation, as well as impairment of the immune responses needed to protect against pathogens and cancer (3–5). Since $CD8^+$ T cells can selectively recognize and kill cancer cells (6), loss of $CD8^+$ T-cell function during aging may have immense consequences on tumor progression.

As critical mediators of antitumor immunity, $CD8^+$ T cells are particularly vulnerable to detrimental age-related changes (7,8). The aging process disrupts repair pathways that maintain cellular integrity and safeguard tissue health, which are needed to preserve the functional capacity of the T-cell compartment (9,10). Furthermore, the total number of $CD8^+$ T cells declines over the human lifetime (11), alongside reduced molecular diversity of T-cell receptors (TCRs) expressed on the surface of existing pools of T lymphocytes (12). As a result, with age, there are fewer naïve T cells available to mount responses against new antigens (13,14). Furthermore, within T cells in aged individuals, genomic instability, mitochondrial dysfunction, impaired proteostasis, senescence, and epigenetic alterations functionally compromise immune activity in response to activation stimuli (10,15–17). These factors contribute to the physiological erosion of T-cell functionality over time (18), and progressively reduce the ability of aged T cells to control infections and tumors, mount vaccine responses, and prevent autoimmunity (19–27).

Although cancer incidence rises steeply with age (28–30), how aging impacts antitumor immunity is still incompletely understood (31,32). Pre-clinical models have yielded mixed results regarding the impact of aging on the directionality and magnitude of tumor growth rates (33–41). However, recent studies in which tumor-bearing animals are treated with immune checkpoint blockade (ICB) therapies that target inhibitory receptors on T cells, have revealed more consistent deficits in aged animals under conditions that provoke antitumor T-cell responses. With only a few exceptions, ICB agents are poorly effective in mice over 16 months of age (35,37,41), suggesting that immune-related deficiencies limit the control of tumors with advanced age.

Here, we set out to uncover how aging changes T cell–mediated immunity against tumors. We found that multiple immunogenic tumors grew more rapidly in aged mice. Aging impaired cytotoxic $CD8^+$ T-cell activation and effector differentiation within the tumor niche, which was due to a striking absence of tumor antigen–specific $CD8^+$ T cells. Providing tumor antigen–specific T-cell clones from young mice to aged mice was sufficient to slow the growth of tumors and sensitized aged animals to PD-1 ICB. These results reveal that progressive decline in the proportion and absolute numbers of tumor-specific T cells may enable tumor outgrowth with age and suggest that loss of tumor antigen–specific T cells may lead to resistance to immunotherapy in some elderly patients. Finally, the substantial reduction in $CD8^+$ T cells that recognize tumor antigens must be considered in future studies that make use of aged mice to model how advanced age intersects with human cancers and other disease states.

MATERIALS AND METHODS

Mice and Cell Lines

Young adult female C57BL/6J wild-type (WT) (RRID:IMSR_JAX:000664), CD45.1 and Tg(TcraTcrb)1100Mjb/J (OT-I) (RRID:IMSR_JAX:003831) mice were purchased from Jackson Laboratories. Young adult female C57BL/6J WT mice were also purchased from Charles River Laboratories. OT-I TCR transgenic mice (RRID:IMSR_JAX:003831) have been previously described (42). Aged mice (20 months or older) were generated in-house or purchased through the National Institutes of Aging (NIA) from Charles River Laboratories. All mice were maintained under identical housing environment and dietary condition. Bedding was transferred between cohorts of young and aged mice 1-2 weeks before tumor implantation. Female mice ages 2-4 months and 20-24 months were used for experiments. All mice were maintained and bred under the guidelines and policies set by the Harvard Medical School Standing Committee on Animals and the National Institutes of Health. All mouse protocols were approved by the Harvard Medical Area Standing Committee on Animals.

MC38 (a gift from Dario Vignali, University of Pittsburg School of Medicine, acquired in 2012) and B16 (a gift from Glen Dranoff, Novartis Institutes for Biomedical Research, acquired in 2012) cell lines were cultured in DMEM (Thermo Fisher Scientific; Cat. No. 11995065) without pyruvate supplemented with 10% FBS and 1% penicillin/streptomycin (Thermo Fisher Scientific; Cat. No. 5140–122). EO771 (purchased from ATCC) cells were cultured in RPMI 1640 (Thermo Fisher Scientific; Cat. No. 11875–119) supplemented with 10% FBS and 1% penicillin/streptomycin (Thermo Fisher Scientific; Cat. No. 5140–122). MC38 and EO771 cell lines were derived from female mice and B16 were derived from male mice. The MC38-OVA and B16-OVA cell lines were generated by transduction with lentiviral supernatants produced from pLX305 plasmid expressing ovalbumin (Addgene ID: 184924) and continuously cultured in complete media containing 2 μg/mL puromycin (Thermo Fisher Scientific; Cat. No. A1113803). The EO771-OVA cell line was generated by transduction with lentiviral supernatants produced from pLX305 plasmid expressing ovalbumin (Addgene ID: 184924 modified by replacing the puromycin resistance gene with a blasticidin resistance gene) and continuously cultured in 5 μg/mL blasticidin (Thermo Fisher Scientific; Cat. No. A1113903). The cells were used for tumor inoculation at 2 to 4 passages after thaw. All cells were cultured at 37°C in a humidified 5% CO_2 incubator. All FBS was heat-inactivated prior to use. No cell line authentication occurred in the past year, and no Mycoplasma testing was performed.

Tumor Experiments

B16, MC38, B16-OVA, and MC38-OVA cells were resuspended in PBS at a concentration of 2.5 x 10^6 cells/mL and 100 μL containing 2.5 x 10^5 cells were subcutaneously injected into the shaved left flanks of young (2-4 months) and aged (20+ months) mice. EO771 and EO771-OVA cells were resuspended in PBS at a concentration of 2.5 x 10^6 cells/mL and 100 μL containing 2.5 x 10^5 cells were injected underneath the nipple in the 4th mammary fat pad. Tumor growth was tracked every 3 days using a caliper, and tumor volumes were calculated using the following formula for ellipsoid volume: 0.5 x L x W x W, where L is the length (longer diameter) and W is the width (shorter diameter). Mice with ulceration or tumors over 2,000 mm^3 were euthanized and recorded as deceased.

For $CD8^+$ T-cell depletion, *InVivoMAb* anti-mouse CD8b (Lyt 3.2) (clone 53-5.8, Cat. No. BE0223, RRID:AB_2687706) and rat IgG1 isotype control (clone HRPN, Cat. No. BE0088, RRID:AB_1107775) were purchased from BioXCell. Isotype control and anti-CD8b (200 µg per mouse) were intraperitoneally injected on days -1, 1, 4, 8, 12 and 16, and blood drawn by cheek bleed on days 3, 10 and 18 to confirm $CD8^+$ T-cell depletion. For experiments involving PD-1 blockade, IgG2a isotype control (clone 2A3, BioXCell, Cat. No. BE0089, RRID:AB_1107769) and anti-PD-1 (clone 29F.1A12, Cat. No. BE0273, RRID:AB_2687796) were purchased from BioXCell. Both IgG2b isotype control and anti-PD-1 were injected intraperitoneally on days 7, 10 and 13 post tumor cell injection (200 µg per mouse).

Adoptive Transfer Experiments

Naïve OT-I $CD8^+$ T cells were isolated from pooled spleens and lymph nodes of young OT-I TCR transgenic mice by negative selection using the Naïve $CD8a^+$ T cell Isolation Kit (Cat No. 130-096-543, Miltenyi Biotec). Flow cytometry for T-cell activation markers was performed to confirm the purity of $CD8^+CD44^-CD62L^+$ T cells prior to infusion. Naïve $CD8a^+$ T cell kit yielded 98.39~99.12% purity. For all adoptive transfer experiments, 10,000 young naïve OT-I T cells in PBS were injected intravenously into young or aged mice one day prior to tumor cell implantation.

Tumor Dissociation and Tumor-Infiltrating Lymphocyte (TIL) Isolation

Tumor, tumor-draining lymph nodes (tdLN), and spleen were harvested on day 12 post tumor injection. Tumors were physically dissociated using the gentleMACS™ Dissociator (Miltenyi) in 1X DPBS containing calcium, magnesium, and 250 units/mL of Type I Collagenase (Cat. No. LS004200, Worthington Biochemical Corporation), followed by enzymatic dissociation at 37°C for 30 minutes. The dissociated tumor cells were filtered through a 70 µm filter, and TILs were enriched using the LSM™ lymphocyte separation medium (Cat. No. 50494, MP Biomedicals). Resuspended tumor cells in PBS, layered above the separation medium, were spun at room temperature for 20 minutes at 800g with the acceleration and brake off. TILs were recovered for further staining. Spleens and tdLN were mechanically dissociated using the 70 µm filter and RBCs in spleens were removed using the Gibco™ ACK Lysing Buffer (Cat. No. A1049201, Fisher Scientific). Final cell products were collected for hemocytometer-based cell counting and flow cytometric staining.

Surface/Intracellular Staining and Flow Cytometry

Primary mouse cells were isolated from spleens, thymus, non-draining inguinal lymph nodes, tdLNs and tumors. Single-cell suspensions were incubated with TruStain FcX (Biolegend) in MACS buffer containing 1X DPBS supplemented with 1% FBS and 2 mM EDTA for 20 minutes on ice to block Fc receptor. Cells were stained using a LIVE/DEAD Fixable Near-IR (ThermoFisher Scientific) or Ghost Dye Violet 510 (Cytek Biosciences) according to the manufacturer's instructions. For surface staining, cells were incubated with fluorophore-conjugated antibodies in MACS buffer solution for 30 minutes on ice. For detection of nuclear proteins, cells were fixed and permeabilized using the Ebioscience FoxP3/Transcription Factor Staining Buffer Set (ThermoFisher Scientific) in accordance with the manufacturer's instructions.

The following antibodies were used: BUV395 Hamster Anti-Mouse TCRβ Chain (BD Biosciences, Clone H57-597), BUV661 Rat Anti-Mouse CD45 (BD Biosciences, Clone 30-F11), BUV496 Rat-Anti-Mouse CD4 (BD Biosciences, Clone GK1.5), BUV805 Rat Anti-Mouse CD8α (BD Biosciences, Clone 53-6.7), eFluor™450 Anti-Mouse Foxp3 (Ebioscience, Clone FJK-16s), Brilliant Violet 510™ Anti-Mouse PD-1 (Biolegend, Clone 29F.1A12), Brilliant Violet 605™ Rat Anti-Mouse CD62L (Biolegend, Clone MEL-14), Brilliant Violet 711™ Anti-Mouse CD366 (Biolegend, Clone RMT3-23), Brilliant Violet 785 ™ Anti-Mouse CD44 (Biolegend, Clone IM7), Alexa Flour 488 Mouse Anti-TCF-7/TCF-1 (BD Biosciences, Clone S33-966), PerCP-Cy5.5 Mouse Anti-Ki-67 (BD Biosciences, Clone B56), PE/Cyanine7 Anti-T-bet (Biolegend, Clone 4B10), Alexa Flour 700 Anti-human/mouse Granzyme-B (Biolegend, Clone QA16A02), H-2Kb MuLV p15E Tetramer-KSPWFTTL-APC (MBL International, TB-M507-2), Tetramer/BV421 - H-2Kb TRP2 SVYDFFVWL (MBL International, TB-5004-4), H-2Db gp100 Tetramer-EGSRNQDWL-PE (MBL International, TS-M546-1), BUV395 Anti-Mouse TCR Vβ3 (BD Biosciences, Clone KJ25), BUV496 Anti-Mouse TCR Vβ5.1/5.2 (BD Biosciences, Clone MR9-4), BUV563 Anti-Mouse CD44 (BD Biosciences, Clone IM7), BUV661 Anti-Mouse TCR Vβ12 (BD Biosciences, Clone MR11-1), BUV737 Anti-Mouse TCR Vβ8.1/8.2 (BD Biosciences, Clone MR5-2), BUV805 Anti-Mouse TCR Vβ10b (BD Biosciences, Clone B21.5), BV421 Anti-Mouse TCR Vβ14 (BD Biosciences, Clone 14-2), BV605 Anti-Mouse TCR Vβ4 (BD Biosciences, Clone KT4), BV650 Anti-Mouse TCR Vβ6 (BD Biosciences, Clone RR4-7), BV711 Anti-Mouse TCR Vβ9 (BD Biosciences, Clone MR10-2), BV750 Anti-Mouse CD3 (BD Biosciences, Clone 145-2C11), BV786 Anti-Mouse TCR Vβ11 (BD Biosciences, Clone RR3-15), FITC Anti-Mouse TCR Vβ7 (BD Biosciences, Clone TR310), RB780 Anti-Mouse CD62L (BD Biosciences, Clone MEL-17), PE Anti-Mouse TCR Vβ8.3 (BD Biosciences, Clone 1B3.3), PE/Fire 700 Anti-Mouse CD4 (BD Biosciences, Clone GK1.5-5), APC Anti-Mouse CD8 (BD Biosciences, Clone 53-6.7), R718 Anti-Mouse TCR Vβ13 (BD Biosciences, Clone MR12-3), and APC-Cy7 Anti-Mouse CD45 (BD Biosciences, Clone 30-F11). H-2Kb chicken ova 257-264 SIINFEKL tetramer was obtained from the NIH Tetramer Core facility. Data collection was performed on a BD FACSymphony cytometer and results were analyzed using FlowJo v10.8.1 (FlowJo LLC, RRID:SCR_008520).

Cytokine Bead Array

Plasma from young and aged mice were freshly acquired from blood in Sodium Heparin-treated BD Vacutainer® plasma tubes (Cat. No. 367874). Blood was centrifuged at 1,500 g for 10 minutes, and plasma was separately aliquoted for flash freezing and immediate storage in −80 °C. Plasma cytokines including IFNγ, IL-6 and IL-12p70 were analyzed using the LEGENDplex Mouse Inflammation Panel cytometric bead array (Cat. No. 740446, BioLegend). Cytokines were measured in accordance with the manufacturer's guidelines.

Single-Cell RNA-Sequencing (RNA-Seq)

$CD8^+$ TILs were enriched through positive selection of bulk $CD8^+$ T cells (Cat. No. 130-116-478, Miltenyi Biotec) from MC38 tumors 12 days post-implantation. Prior to magnetic enrichment, MC38 tumors were minced in RPMI containing 2% FBS, 2 mg/mL collagenase P (Roche), and 50 mg/mL DNase I (Sigma) and then incubated at 37 °C with gentle rocking for 10 minutes. $CD8^+$ T cells were magnetically enriched by positive selection at 4 °C and then incubated in 50 mL of blocking buffer for 10 minutes on ice, where the blocking buffer contained 1:100 dilution of TruStain FcX PLUS (Cat. No. 156604, BioLegend) prepared in Cell Staining

Buffer (Cat. No. 420201, BioLegend). Hashing antibodies were prepared by diluting TotalSeq-B antibodies (Cat. No. 155831, 155833, 155835, 155837; BioLegend) 1:50 in Cell Staining Buffer (Cat. No. 420201, BioLegend) and incubating for 30 minutes on ice. Cells were washed three times in RPMI containing 2% FBS, with a total volume of 3.5 mL per wash, passing the resulting cell suspension through a 30-micron filter before the final wash. Live cells were counted on a CytoFLEX after staining with 7-AAD (Cat. No. 420404, BioLegend). For a target recovery of 4,000 single cells per mouse, 6,400-7,000 live cells per mouse were loaded per well onto the Chromium Controller (10X genomics) and processed according to the manufacturer's instructions (10X Genomics, Chromium - Single Cell 3' Reagent Kits v2). Hashed TILs from 3-4 different mice were pooled per 10X sample. All samples were sequenced on an Illumina NextSeq500 sequencer using a 75-bp kit with paired-end reads.

Single-Cell RNA-Seq Bioinformatics Analysis

Sample demultiplexing, barcode processing, alignment, filtering, and unique molecular identifier (UMI) counting were performed using the Cell Ranger analysis pipeline (v.4.0.0). Counts were subsequently used for downstream analysis. Data pre-processing, normalization, integration, and clustering was performed using the Seurat package (v.3.2.3) (RRID:SCR_016341) (43) in R (v.4.0.3 "Bunny-Wunnies Freak Out") (RRID:SCR_001905). For each sample, genes expressed in fewer than three cells were excluded. For each sample, cells with poor quality metrics were removed by the following criteria: fewer than 200 unique genes, greater than 6,000 unique genes, greater than 10% mitochondrial counts. Cells were further removed when demultiplexing samples by hashtag oligo expression, utilizing the demultiplexing method implemented by the `HTODemux` function implemented in the Seurat package. The optimal quantile value was determined separately for each sample by testing a range of quantile values between 0.90 and 0.99 in 0.01 step intervals and selecting the quantile value which kept the largest number of singlets. Cells called as negative or doublets by hashtag oligo demultiplexing were excluded. All samples were then merged into a single Seurat object. Normalization and variance stabilization was performed using the R package `sctransform` (v.0.3.3), which interfaces directly with Seurat, on each sample separately (44). Dimensionality reduction and clustering were performed using Seurat's standard clustering workflow, utilizing the functions `FindVariableFeatures`, `RunPCA` and then `RunUMAP`. Where applicable, the first 30 principal components were utilized. Unsupervised clustering was performed utilizing the `FindNeighbors` and `FindClusters` functions. We tested several resolutions of clustering, from 0.1 to 0.9 in 0.1 step intervals and selected a clustering resolution based on the correspondence of clusters with known biological markers. Cells bearing $CD8^+$ T-cell markers (CD8A, CD8B, and CD3E) were subsetted from the Seurat object and the Seurat workflow was rerun using the same methodology of the full dataset, starting from normalization and variance stabilization using `sctransform` to unsupervised clustering. The resulting expression matrix contained 11,634 cells by 21,253 genes, with 8,081 cells derived from tumors implanted in young adult mice and 3,553 cells from tumors implanted in aged mice. Differential expression analysis between clusters and comparing age conditions were performed using a Wilcoxon rank sum test, utilizing the `FindMarkers` or `FindConservedMarkers` functions as appropriate.

Cancer Single-cell Expression Map Analysis

Harmonized cell subtype information and metadata were downloaded from the Cancer Single-cell Expression Map online database (https://ngdc.cncb.ac.cn/cancerscem/) (45). Samples were filtered to include only patients with solid tumors and metadata for diagnosis age (n = 62). Cell types were pruned to retain immune populations only: $CD8^+$ naïve T cells, $CD8^+$ effector memory T cells (Tem), $CD8^+$ central memory T cells (Tcm), $CD8^+$ effector T cells, $CD4^+$ naïve T cells, $CD4^+$ Tem, $CD4^+$ Tcm, $CD4^+$ effector T cells, regulatory T cells (Tregs), Naïve B cells, Memory B cells, Dendritic cells (DC), natural killer (NK) cells, Mast cells, Macrophages, Plasma cells, Activated B cells, Monocytes, and Neutrophils. Calculated parameters from the resulting datasets include the following: % NK cells of total, % B cells of total, % Macrophages of total, % DCs of total, % Mast cells of total, % Plasma cells of total, % Monocytes of total, % $CD3^+$ T cells of total, % $CD4^+$ T cells of total, % $CD8^+$ T cells of total, % $CD8^+$ of $CD3^+$, % Effector of $CD8^+$, % Tem of $CD8^+$, % Tcm of $CD8^+$, % $CD4^+$ of $CD3^+$, % Treg of $CD4^+$, Treg to $CD8^+$ ratio, % Effector of $CD4^+$, % Tem of $CD4^+$, and % Tcm of $CD4^+$. Spearman correlation coefficients and statistical significance were calculated using the rcorr function from the Hmisc (v5.0-1) (RRID:SCR_022497) R package.

TCGA Survival Analysis.

For survival analysis, input gene expression data and clinical metadata for Diagnosis Age were downloaded from the cBioPortal website, selecting patient samples associated with "TCGA PanCancer Atlas Studies". Gene expression data were downloaded in "mRNA Expression, RSEM (Batch normalized from Illumina HiSeq_RNASeqV2)" format. The resulting dataset was filtered to keep only primary tumor samples with both diagnosis age metadata and transcriptomic data (n = 9,286). RSEM (RNA-Seq by Expectation-Maximization)-normalized values were first log2-transformed, and then centered and scaled within each cancer type. Immune signature scores were calculated per patient as the mean of scaled gene expression within each gene set (46,47). Clinical outcome endpoints for each patient were taken from a standardized dataset named the "TCGA Pan-Cancer Clinical Data Resource" (48). Survival analysis was performed in R on patient samples with both transcriptomic data and survival metadata (n = 9.266) using the survival R package (v3.5-5) (RRID:SCR_021137) using quartile cut-offs (bottom 75% versus top 25%), and survival graphs were generated using the survminer package (v0.4.9) (RRID:SCR_021094) in R.

TCR Vβ Analysis

TCR Vβ analysis was performed on $CD8^+$ T cells isolated from thymus, spleen, tdLN, non-draining lymph node, and tumor bed from female C57BL/6J mice bearing B16-OVA tumors at 2, 8, 12, 16, and 20-months of age. All tissues were harvested 12 days post-implantation. TCR Vβ usage was determined by staining with a panel of 13 fluorescently labeled antibodies that recognize different murine Vβ chains, where clones and colors are listed in the "*Surface/Intracellular Staining and Flow Cytometry*" section. Coefficients of variation for individual TCR Vβ chains were calculated as the standard deviation divided by the mean for the frequency of that chain among all $CD8^+$ T cells resolved by differentiation state, age, and tissue site. Shannon Diversity Index was calculated in R using the vegan R package (2.6-4) (RRID:SCR_011950).

Statistical Analysis

Statistics were computed with GraphPad Prism 9 software (GraphPad Software Inc., RRID:SCR_002798) using unpaired Student's t-test for comparisons between two groups and two-way ANOVA for tumor growth kinetics with multiple variables, followed by the Bonferroni Post-Hoc test for comparison of tumor sizes at multiple individual time points. Graphs containing tumor growth curves represent mean values with error bars representing the Standard Error of the Mean (SEM). Unless noted otherwise, all other data are represented as mean +/- SEM. P-values are denoted in figures as: *p<0.05, **p<0.01, ***p<0.001, ****<0.0001. Most figures are representative of two independent experiments.

Data and code availability

All code used to process the single-cell RNA-seq data can be found on GitHub at https://github.com/hms-sharpies/aged-TIL-scRNAseq. Raw and processed single-cell RNA-seq data files were uploaded to the NCBI GEO repository (accession: GSE236227) and the Single Cell Portal (accession: SCP2091).

RESULTS

Aging attenuates tumor growth control across multiple syngeneic cancer models

To evaluate the overall impact of aging on tumor outgrowth, we implanted syngeneic cancer cells in immunocompetent mice and monitored tumor size, comparing young mature adult (2-4 months) and aged (20-24 months) recipient mice. Our aged cohorts are approximately equivalent to humans at ~65 years of age, when cancer incidence rises sharply (28–30,49). When comparing mice of these ages, aged C57BL/6J mice are heavier (**Supplementary Fig. S1A**) and have elevated levels of circulating inflammatory cytokines (**Supplementary Fig. S1B-D**), which is a hallmark of immunological aging in humans (2,10,32). We initially tested three cancer models (subcutaneous MC38, colorectal, orthotopic EO771, breast, and orthotopic B16, melanoma), which differ by tissue of origin, molecular drivers, and immunogenicity. In highly immunogenic MC38 and EO771 tumors, we observed more rapid tumor outgrowth in aged animals, resulting in larger tumors (**Fig. 1A, Supplementary Fig. S1E**). Conversely, less immunogenic B16 cell lines grew at similar rates in young adult versus aged mice (**Fig. 1A, Supplementary Fig. S1E**). Expressing hen egg white ovalbumin (OVA), a protein that harbors the potent $CD8^+$ T-cell antigenic peptide SIINFEKL, in MC38 and EO771 cell lines further amplified the increase in tumor growth rate and reduced survivorship during aging (**Fig. 1B-C, Supplementary Fig. S1F**). Whereas B16 tumors grow at the same rate in young adult versus aged animals (**Fig. 1A**), B16-OVA tumors with enhanced immunogenicity grow more aggressively in elderly hosts, reflected in both growth kinetics and survival (**Fig. 1B-C, Supplementary Fig. S1F**).

We tested directly whether the presence of $CD8^+$ T cells altered tumor growth kinetics in aged animals. We depleted $CD8^+$ T cells systemically in MC38 or EO771 tumor–bearing animals using antibody treatment, which significantly reduced circulating $CD8^+$ T-cell frequencies (**Supplementary Fig. S1G-K**). In young adult but not aged hosts, $CD8^+$ T-cell

depletion significantly accelerated tumor growth rate (**Fig. 1D-E**). Together, these results suggest that functional deficits in $CD8^+$ T cells during aging causally increase tumor outgrowth.

Aging is associated with dysfunctional tumor-infiltrating $CD8^+$ T cells

Next, we performed flow cytometry to profile how aging changes the infiltration of T cells within tumors. We compared immune cells isolated from growing tumors versus tdLN. Consistent with previous reports that aging leads to a contraction in lymphocyte pools (11,18), we observed reduced total $CD3^+$ T-cell numbers and frequencies relative to all $CD45^+$ leukocytes in tdLN across all three tumor models, including a significant reduction in the proportion of naïve $CD8^+$ T cells (**Supplementary Fig. S2A-C**). However, frequencies and absolute numbers of T lymphocytes inside tumors were not altered by aging (**Supplementary Fig. S2A-B**). We observed similar changes specifically within $CD8^+$ T cells, where the total numbers and frequencies relative to $CD45^+$ leukocytes were not significantly altered within tumors, despite changes in tdLN, including a significant reduction in tdLN absolute numbers across all three models (**Supplementary Fig. S2D-E**). Therefore, we conclude that $CD8^+$ T cells infiltrate tumors to the same extent in young adult versus aged host animals.

To probe the functional state of the aged $CD8^+$ T-cell compartment, we assessed immune markers associated with $CD8^+$ T-cell activation, differentiation, and cytotoxicity by multiparameter flow cytometry. Consistent with a defect in activation, a smaller proportion of intratumoral $CD8^+$ T cells in aged mice expressed both CD44 and PD-1, which are markers of antigen experience (CD44) and activation/exhaustion (PD-1), respectively (**Fig. 2A**). Within aged intratumoral $CD44^+PD\text{-}1^+CD8^+$ T cells, we observed a reduction in the proportion of cells expressing markers associated with exhaustion, including high expression of the inhibitory receptor TIM3 and low expression of the transcription factor TCF1 **(Fig. 2B).** Reciprocally, the proportions and absolute numbers of cells expressing markers associated with a progenitor-exhausted T-cell state ($TIM3^-TCF^+$) were increased in tumors from aged as compared to young hosts (**Supplementary Fig. S2F**). While there were fewer intratumoral effector memory $CD8^+$ T cells in aged mice, proportions of intratumoral central memory $CD8^+$ T cells were increased (**Fig. 2C, Supplementary Fig. S2G).** Overall, these results suggest that aging impairs $CD8^+$ T cell activation and differentiation within tumors.

We also observed that aging reduced key indicators of proliferation and effector differentiation. For example, significantly fewer aged intratumoral $CD8^+$ T cells expressed the transcription factor T-BET (**Fig. 2D**), which plays an important role coordinating the generation of cytotoxic effector $CD8^+$ T cells (50,51). In addition, aged $CD8^+$ T cells within tumors expressed lower levels of the cytotoxic protein Granzyme-B (GZMB) as well as MKI67, a marker of proliferation (**Fig. 2E-F**). Although aging increased the proportion of $CD8^+$ T cells expressing T-BET, MKI67 and CD44 within tdLN, the absolute numbers of $CD8^+$ T cells expressing these markers were reduced or comparable across all three models in aged mice compared to young mice (**Supplementary Fig. S2H-J**). Thus, while the impact of aging on peripheral T cells is complex, we observed major functional deficits within intratumoral $CD8^+$ T cells in aged animals.

In addition, we explored whether expansion of suppressive regulatory $CD4^+$ T cells might promote $CD8^+$ T-cell dysfunction in tumors from aged animals. In the tdLN, the frequencies of $CD4^+$ T cells relative to $CD3^+$ T lymphocytes were not significantly altered (**Supplementary Fig.**

S2K). In contrast, absolute numbers of $CD4^+$ T cells were significantly decreased in the tdLN across all models (**Supplementary Fig. S2L)**. There was a large increase in the frequency of $FOXP3^+$ Tregs in the tdLN (**Supplementary Fig. S2M-N**), which reduced the overall ratio of $CD8^+$ to regulatory T cells, a hallmark of immunosuppression, in the tdLN (**Supplementary Fig. S2O**). These effects were absent in the tumor bed, where aging instead reduced the proportion of FOXP3-expressing $CD4^+$ T cells (**Supplementary Fig. S2M**). Therefore, accelerated tumor outgrowth in aged animals (**Fig. 1A-B**) cannot be explained solely by increased accumulation of Tregs.

Finally, to examine whether altered antigen presentation by myeloid cells contributes to $CD8^+$ T-cell dysfunction, we examined quantitative and qualitative changes in the myeloid-cell compartment within the tdLN and tumor of aged mice. The proportion of $CD11B^+$ myeloid cells increased in tdLN of aged mice (**Supplementary Fig. S3A**). Amongst $CD45^+$ cells, the proportion of macrophage, monocytes, $GR\text{-}1^+$ myeloid cells and $CD11C^-$ DCs in tdLN increased with age (**Supplementary Fig. S3B**). Furthermore, aged myeloid cells in the tdLN and tumor bed, including macrophages, DCs and monocytes expressed higher levels of SIINFEKL-peptide presented on MHC class I (**Supplementary Fig. S3C-D**). Moreover, DCs expressed comparable levels of CD40 (**Supplementary Fig. S3E**) and higher levels of co-stimulatory molecule CD80 (**Supplementary Fig. S3F**) in the tdLN of aged as compared to young adult hosts. Aged DCs also expressed higher levels of inhibitory programmed cell death ligand 1 (PD-L1) (**Supplementary Fig. S3G**) in the tdLN. Thus, antigen-presenting cells in aged mice express molecules that can prime tumor-specific T cells.

Collectively, these results indicate that aging leads to marked deficits in the activation, effector differentiation, and functional status of intratumoral $CD8^+$ T cells, despite enhanced antigen presentation and heightened co-stimulatory molecule expression in the tdLN.

Single-cell RNA-Seq analysis reveals deficits in $CD8^+$ T-cell differentiation within aged tumors

Since activation markers were reduced in intratumoral $CD8^+$ T cells with advanced age, we performed single-cell RNA-Seq to examine age-associated T-cell dysfunction in molecular detail (**Fig. 3A**). We first enriched tumor-infiltrating $CD8^+$ T cells from MC38 tumors implanted in young adult or aged animals. Next, we barcoded samples with hashing antibodies to associate individual cells with specific donor animals, and then performed single-cell transcriptomic analysis. After dimensional reduction and unsupervised clustering, this yielded a single cell dataset with transcriptomes barcoded by mouse (**Supplementary Fig. S4A-C**) grouped into seven clusters (**Fig. 3B**). Each cluster was annotated based on the expression of gene markers for differentiation and functionality (**Fig. 3B, Supplementary Fig. S4D-I**). While each cluster contained cells from both young adult and aged tumors (**Supplementary Fig. S4I**), we identified cell states that were disproportionately represented per condition (**Fig. 3C-D**). Clusters #2 and #3, representing progenitor exhausted and naïve T cells, were populated to a greater extent by aged $CD8^+$ T cells, although the increase in naïve T cells was not statistically significant. Consistent with our flow cytometry profiling studies, clusters #0, #1, and #4, representing transitory exhausted, progenitor exhausted/interferon-sensing, and terminally exhausted cell populations, were enriched for cells isolated from young adult animals (**Fig. 3D**). To probe the underlying landscape of this dataset, we scored each cluster on gene sets reflecting T-cell quiescence or stimulation (**Supplementary Fig. S4J-L**) and then ordered the clusters by the

two signature scores (**Fig. 3E**). Clusters with high quiescence and low stimulation scores contained the highest number of differentially expressed transcripts by age, which became progressively lower in clusters with low quiescence and high stimulation scores (**Fig. 3E**). Therefore, we identified transcriptional differences that negatively associated with T-cell stimulation state.

Next, we performed trajectory analysis to test whether T-cell fates within tumors are distinct in the aged microenvironment. We identified a consistent trajectory between young adult and aged $CD8^+$ T cells (**Fig. 3F**), indicating that the overall architecture of T-cell differentiation is similar between the two conditions. Individual clusters mapped to distinct relative positions along the reconstructed trajectory (**Supplementary Fig. S4M-S**), which captured a progression of cell states associated with T-cell differentiation. Naïve cells in cluster #3 (**Supplementary Fig. S4P**) anchored one end of the trajectory, whereas proliferating T cells in cluster #5 (**Supplementary Fig. S4R**) mapped to the other end. All other clusters were located at intermediate positions along the pseudotime trajectory (**Supplementary Fig. S4M-S**). Consistent with the differences in representation of young adult or aged T cells across clusters, T cells from young mice were distributed across the entire trajectory (**Fig. 3G**), whereas aged T cells were crowded toward the naïve end of the trajectory (**Fig. 3H**) that contained cells from Clusters #1, 2, 3, and 6 (**Fig. 3I, Supplementary Fig. S4T**). Collectively, these results reveal a common differentiation trajectory for $CD8^+$ T cells that enter tumors in young adult versus aged animals, but far fewer $CD8^+$ T cells in activated cell states with advanced age.

Tumor-specific $CD8^+$ T-cell clones are diminished in aged mice

During acute viral infection, aged animals exhibit an up to 10-fold decrease in antigen-specific viral precursor $CD8^+$ T cells, which results in poor antiviral responses (19,20). Given that antigen recognition is absolutely required for antitumor T-cell responses, we reasoned that decreased numbers of naïve and tumor-reactive $CD8^+$ T cells may account for the rapid outgrowth of tumors in aged animals. Consistent with this hypothesis, peripheral naive $CD44^-$ $CD62L^+CD8^+$ T cells were markedly decreased across all three tumor models (**Fig. S2C**). To identify tumor antigen–specific $CD8^+$ T cells, we implanted OVA-expressing MC38, B16, and EO771 syngeneic tumor cell lines into young adult or aged animals and used fluorescently labeled MHC-tetramer reagents that bind to SIINFEKL-reactive $CD8^+$ T cells, to label OVA-specific T cells from tumors. SIINFEKL-reactive $CD8^+$ T cells were readily detected in day 12 tumors from young mice across all three models. However, tumors implanted in aged mice were virtually devoid of SIINFEKL-reactive $CD8^+$ T cells (**Fig. 4A-C, Supplementary Fig. S5A-B**). This deficiency was reflected both at the level of proportion and absolute cell numbers in the tumors from aged as compared to young adult animals (**Fig. 4D-E**). Similarly, the absolute number of SIINFEKL-reactive $CD8^+$ T cells was decreased in tdLNs from aged versus young adult animals (**Supplementary Fig. S5C**).

Since OVA is a strong model antigen, we next examined whether $CD8^+$ T cells reactive toward endogenous tumor-associated antigens in B16-OVA cell lines also declined with age. Consistent with the decline in SIINFEKL-reactive $CD8^+$ T cells, aged B16-OVA tumor-bearing mice exhibited a significant reduction in the proportion and absolute numbers of intratumoral $CD8^+$ T cells reactive against epitopes derived from classical melanoma tumor antigens, including MuLV p15E, gp100, and TRP-2 (**Fig. 4F-G, Supplementary Fig. S5D-G**) (52). As

observed with SIINFEKL-reactive CD8$^+$ T cells, the numbers of tdLN CD8$^+$ T cells reactive against MuLV p15E, gp100 and TRP-2 antigen were significantly reduced in aged as compared to young B16-OVA tumor-bearing mice (**Supplementary Fig. S5D**). Lastly, the drop in SIINFEKL-reactive CD8$^+$ T cells in aged tumor-bearing mice could not be attributed to T cell survival differences, as viability was comparable between bulk CD3$^+$, bulk CD8$^+$ and SIINFEKL-reactive intratumoral CD8$^+$ T-cell populations (**Supplementary Fig S5H-J**). Consistently, TCRβ expression levels were comparable between young adult and aged tumor-infiltrating CD8$^+$ T cells (**Supplementary Fig S5K**). Taken together, these results suggest that a lack of tumor antigen–specific T cells may represent a critical barrier for the generation of effective antitumor immunity in aged hosts.

TCR Vβ usage changes with advanced age and results in decreased TCR diversity

Each T cell carries uniquely recombined α- and β-chains genes that comprise the TCR, which enables the adaptive immune system to recognize a broad array of antigens. The β-chain is composed of variable (V), joining (J), and constant (C) gene segments. Mature T cells express a single Vβ segment selected from 31 possible V segment gene subfamilies that are rearranged during T-cell development, such that Vβ usage can be used as a proxy for T-cell diversity (53). To evaluate how TCR diversity changes over lifespan, we measured TCR Vβ usage by T cells, which can be distinguished by flow cytometry after surface staining with antibodies for the different Vβ chains, in multiple tissue sites and at multiple timepoints.

We profiled CD8$^+$ T cells across five distinct tissue sites (thymus, spleen, inguinal non-draining lymph node, tumor-draining lymph node, and tumor) and five ages (2, 8, 12, 16, and 20 months of age) from mice bearing B16-OVA tumors after 12 days of growth (**Supplementary Fig. S6A-K**). First, we determined the frequency of CD8 single-positive thymocytes (**Supplementary Fig. S6A**) and intratumoral CD8$^+$ T cells (**Supplementary Fig. S6B**) expressing 13 common Vβ genes. Within the tdLN, inguinal non-draining lymph node and spleen we additionally examined TCR Vβ usage within the naïve (CD62L$^+$CD44$^-$), central memory (CD62L$^+$CD44$^+$), and effector memory (CD62L$^-$ CD44$^+$) CD8$^+$ T-cell compartments across the five age groups (**Supplementary Fig. S6C-K**). We first determined how Vβ usage changes with advancing age. In the young adult setting (2 months), the pattern of Vβ expression was consistent between animals, where T cells isolated from the same tissue site were the most similar (representative bar plots for 2 months shown in **Supplementary Fig. S6A-K**). Within tumors, this pattern became more variable between animals, likely due to clonal expansion of T cells with specificity for tumor antigens (**Supplementary Fig. S6B**). Similar results were seen at 8-, 12-, and 16-months of age (**Supplementary Fig. S6B**), but between 16- and 20-months of age, there was a notable change. The central memory pool became dominated by single Vβ chains in the spleen and lymph nodes, consistent with the creation of T-cell memory (**Supplementary Fig. S6C-E**). However, variation between mice increased, where some animals retained young adult patterns of Vβ usage and others did not (**Supplementary Fig. S6C-E**). In addition, Vβ expression in naïve T cells was also impacted, where mice >20 months of age exhibited greater variation overall, and some were dominated by the expression of a single Vβ gene, particularly in the spleen (**Supplementary Fig. S6F-H**). Among naïve cells, this may be due to stochastic attrition of T-cell clones, as patterns of thymic Vβ expression were less impacted by advanced age (**Supplementary Fig. S6A**). In summary, we reveal a qualitative age-dependent shift in Vβ usage among CD8$^+$ T cells.

To quantify variation in Vβ usage, we calculated coefficients of variation (CV) for each Vβ gene. This analysis confirmed that heterogeneity among Vβ usage for thymic $CD8^+$ T cells remained similar across age brackets (**Fig. 5A**). By contrast, naïve $CD8^+$ T cells in the spleen, tdLN, and tumor bed became significantly more variable at 20 months of age (**Fig. 5B-D**). This was associated with a reduction of diversity in Vβ usage. Whereas age had no impact on the Shannon diversity coefficient for thymic $CD8^+$ T cells (**Fig. 5E**), the Shannon diversity coefficient was reduced significantly above 20 months of age in the spleen, tdLN, and tumor bed (**Fig. 5F-H**). These findings suggest that aging primarily impacts the peripheral T-cell pool, leading to a less diverse TCR repertoire.

We next evaluated how frequencies of $CD8^+$ T cells that recognize two distinct model antigens, SIINFEKL (derived from ovalbumin) and TRP-2 (derived from an endogenous melanocyte-associated antigen) change over the lifespan of a mouse. This is important because the availability of T cells that recognize tumor antigens is required to initiate an adaptive immune response against developing tumors. We implanted B16-OVA tumors into wild-type mice across ages, ranging from 2 months (where most tumor immunology studies are performed) to 20 months old, evaluating antigen-specific $CD8^+$ T-cell responses on 12 days post-implantation. Consistent with our previous findings, frequencies of intratumoral bulk $CD8^+$ T cells remained constant across lifespan (**Supplementary Fig. S6L-M**). In contrast to minor changes in the tdNL (**Fig. 5I-J**), $CD8^+$ T cells recognizing either SIINFEKL or TRP-2 tetramer reagents progressively dropped in frequency in the tumor over lifespan (**Fig. 5K-L**). This happened earlier among SIINFEKL-reactive $CD8^+$ T cells, which started declining at 8 months of age, and were nearly absent by 20 months of age (**Fig. 5K**). This decline coincided with the timeframe of thymic involution (**Supplementary Fig. S6N**). In contrast, while $CD8^+$ T cells recognizing TRP-2 similarly declined over lifespan, a measurable fraction could be detected even at 20 months of age (**Fig. 5L**). We observed key differences in functional correlates of cytotoxicity and activation markers between the two types of antigen-specific $CD8^+$ T cells. Across all ages where SIINFEKL-reactive $CD8^+$ T cells could be detected inside tumors, they maintained similar levels of Granzyme B expression (**Fig. 5M**). In contrast, the proportion of TRP-2–reactive $CD8^+$ T cells that expressed Granzyme B declined progressively across lifespan (**Fig. 5N**). We observed similar frequencies of SIINFEKL-reactive $TIM3^+PD\text{-}1^+CD8^+$ T cells within tumors across all ages while the proportion of these cells among TRP-2–reactive $CD8^+$ T cells declined progressively with increased age (**Fig. 5O-P**). These findings indicate that T cells with specificity for different tumor antigens decline with distinct kinetics over lifespan, which we believe was previously unappreciated.

Restoring antigen-specific $CD8^+$ T cells improves tumor control in aged mice

To determine whether declining frequencies and numbers of tumor-specific T cells causally increase tumor outgrowth with advanced age, we tested if providing tumor antigen–specific $CD8^+$ T cells to aged mice would be sufficient to slow the growth of implanted tumors. We adoptively transferred naïve young OT-I $CD8^+$ T cells, which express a fixed TCR that recognizes the SIINFEKL peptide, into young adult or aged animals prior to B16-OVA tumor cell implantation (**Fig. 6A**). Adoptive transfer of OT-I $CD8^+$ T cells significantly slowed tumor growth in both young adult and aged recipients during the first 20 days (**Fig. 6B, Supplementary Fig. S7A**). At early time points, OT-I T cells slowed tumor growth to a greater extent in aged animals

compared to young animals (**Fig. 6C**). However, tumors implanted in aged mice ultimately escaped immune control (**Fig. 6B-C**). Consistent with these findings, marginal differences were observed in the overall survival between PBS and OT-I treated aged animals, whereas OT-I transfer resulted in long-term survival in 25% of young adult animals (**Fig. 6D**). These results indicate that OT-I $CD8^+$ T cells originating from young adult animals can induce antitumor activity but fail to elicit durable antitumor responses in aged recipients.

To examine the cellular fate of adoptively transferred OT-I T cells, we transferred congenically distinct naïve young $CD45.1^{+/+}$ OT-I $CD8^+$ T cells into young adult or aged $CD45.2^{+/+}$ recipients, and subsequently challenged these mice with B16-OVA or MC38-OVA tumor cells. At day 12 following tumor cell inoculation, the proportions, and absolute numbers of OT-I $CD8^+$ T cells were increased in the tdLN of aged as compared to young adult recipients in both tumor models, whereas the proportion of tumor-infiltrating OT-I T cells was reduced (B16-OVA) or comparable (MC38-OVA) with advanced age (**Fig. 6E-F**). To assess the proliferation and activation state of the transferred T cells, we measured MKI67, PD-1 and T-BET expression within the $CD45.1^{+/+}$ OT-I T-cell fraction. In tdLN of aged recipients, there were significantly elevated proportions of transferred T cells expressing these markers (**Fig. 6G-H**), with the exception of T-BET in B16-OVA, whereas the proportions of tumor-infiltrating $MKI67^+$, $PD\text{-}1^+$ and $T\text{-}BET^+$ cells were comparable between young adult and aged recipients (**Fig. 6I-J**). The proportion of $PD\text{-}1^+$ OT-I cells expressing markers associated with the progenitor exhausted ($TIM3^-TCF1^+$) and more terminally exhausted cell states ($TIM3^+TCF1^-$) were also comparable between young and aged tumors (**Supplementary Fig. S7B**). These results suggest that the function of tumor-infiltrating OT-I $CD8^+$ T cells is comparable in aged recipients on day 12 and that the aged environment induces heightened activation of these cells in the tdLN.

Providing tumor-specific T-cell clones synergizes with PD-1 blockade in aged mice

Since ICB therapies re-invigorate antitumor $CD8^+$ T-cell responses, we predicted that aged mice would respond poorly to ICB, due to deficits in tumor-matching clones. We therefore tested whether aged mice were resistant to anti-PD-1 ICB (**Supplementary Fig. S7D**). Whereas administering anti-PD-1 therapy to B16-OVA or MC38-OVA tumor-bearing young animals induced potent antitumor activity, aged animals did not respond (**Fig. 6K, Supplementary Fig. S7D-G**). Consistent with these results, overall survival was significantly extended in young adult, but not aged animals treated with anti-PD-1 therapy (**Fig. 6K, Supplementary Fig. S7E**). To elucidate whether deficits in tumor-reactive T-cell clones limited the efficacy of ICB in aged animals, we evaluated whether adoptive transfer of young adult OT-I T cells could sensitize aged animals to anti-PD-1 therapy (**Fig. 6L**). In young mice, administration of either OT-I T cells or anti-PD-1 monotherapy resulted in a comparable therapeutic response (**Fig. 6M, Supplementary Fig. S7H**). Administration of OT-I T cells followed by anti-PD-1 therapy in young adult animals resulted in robust antitumor activity characterized by complete tumor clearance in 7 out of 8 mice (**Fig. 6M, Supplementary Fig. S7H**). In the aged setting, adoptive transfer of OT-I T cells followed by anti-PD-1 therapy elicited more effective tumor control in comparison to adoptive transfer of OT-I $CD8^+$ T cells alone (**Fig. 6N, Supplementary Fig. S7H**) and significantly prolonged survival of aged tumor-bearing mice, although the percentage of long-term survivors was much less than in young mice (**Fig. 6N**). These results demonstrate that lack of tumor-antigen specific T cells limit responses to ICB in aged mice.

Aging is associated with attenuated CD8$^+$ T-cell function in human cancer

To determine whether intratumoral CD8$^+$ T cells decline with age in humans, we performed bioinformatics analysis on transcriptomic datasets from cancer patients. First, we tested whether CD8$^+$ T-cell infiltration changes with diagnosis age across ~10,000 patient tumors sequenced through TCGA. We scored each patient sample against a gene signature consisting of markers for CD8$^+$ T-cell lineage and cytotoxicity (47) as a proxy for T-cell infiltration. After binning patients by diagnosis age, we found that the T-cell infiltration score remained constant across age brackets (**Fig. 7A**), in agreement with our data in pre-clinical mouse tumor models (**Supplementary Fig. S2A-F**) as well as previous studies (54).

Next, we evaluated whether aging altered the frequency of the effector subset of CD8$^+$ T cells, which are critical for tumor control by the immune system, in the tumor niche. We analyzed single-cell RNA-Seq samples aggregated through the Cancer Single-Cell Expression Map (SCEM) (45), which includes harmonized cell type annotations that enable the comparison of key cell populations across multiple independent studies. After curating patient samples from primary solid tumors, we then calculated Spearman correlation coefficients between immune cell frequencies and diagnosis age (**Fig. 7B-C**). Overall, plasma cells were the only major population that significantly declined with age (**Fig. 7B**), while frequencies of T lymphocytes (total CD3$^+$ cells and CD4$^+$ T cells) significantly increased with diagnosis age (**Fig. 7B**). Within intratumoral CD3$^+$ lymphocytes, however, we identified specific deficits in CD8$^+$ T cells. While total CD8$^+$ T-cell frequencies were unchanged (**Fig. 7A-B**), the proportion of CD8$^+$ effector T cells significantly declined with diagnosis age (**Fig. 7C-D**), leading us to hypothesize that the CD8$^+$ T cells present in aged patients are less effective at controlling tumors.

Finally, we asked whether CD8$^+$ T-cell infiltration was predictive for survival in young versus aged patients using TCGA datasets. Since TCGA contains >30 different cancer types, each with a distinct distribution of diagnosis ages (**Supplementary Fig. S8A**), we controlled for tumor representation by separating patients into aged (oldest 25%) or young (youngest 75%) groups by quantiles calculated within each cancer type. Likewise, to control for differences in T-cell infiltration linked to tumor origin, we divided each patient into CD8$^+$ T cell–high or –low groups per cancer type using the same gene signature as in **Fig. 7A**. This approach resulted in an even distribution of cancer types between young versus aged patients as well as inflamed versus non-inflamed samples (**Supplementary Fig. S8B**), which we then used for survival analysis with outcomes and endpoints from the TCGA-Clinical Data Resource (CDR) (48). Although overall survival (OS) very strongly and significantly stratified by diagnosis age (**Supplementary Fig. S8C**), progression-free interval (PFI) was more similar between the two groups (**Supplementary Fig. S8D-E**). Therefore, we evaluated the effect of CD8$^+$ T-cell tumor infiltration on PFI in young versus aged patients. Among the youngest 75% of patients, PFI was significantly longer in individuals with a high CD8$^+$ T-cell score (**Fig. 7E**). By contrast, T-cell score failed to stratify PFI for aged patients (**Fig. 7F**). Finally, we applied gene signatures reporting on major immune subsets found in tumors in this survival analysis to probe how aging changes immune-mediated determinants of cancer progression. Among young patients only, a high CD8$^+$ T-cell score significantly was associated with extended median patient PFI using two different gene signatures (**Fig. 7G**) (46,47). Likewise, a B-cell gene signature yielded the same pattern as CD8$^+$ T cells on cancer progression, but with smaller effect size (**Fig. 7G**). Conversely, Th2 cells were associated with reduced PFI and had a far larger effect size in aged

patients (**Fig. 7G**). Together, this analysis suggests that aging changes how the immune system controls a developing tumor with consequences on patient survival.

DISCUSSION

Aging is one of the primary risk factors for developing cancer. Since progressive decline of the adaptive immune system is an established hallmark of aging, a better understanding of how immune aging intersects with tumor progression has widespread implications for human health. Here, we have systematically and comprehensively assessed how aging impacts antitumor $CD8^+$ T-cell responses across three different mouse cancer models. Our studies identify loss of tumor antigen–specific $CD8^+$ T cells as a common driver of disease progression with age. This finding places TCR diversity central to healthy aging and as an essential determinant of effective anti-tumor activity.

Given that T cells are the primary cell type that responds to ICB therapy, age-related loss of tumor-specific T cells may substantially limit the efficacy of ICB in elderly patients. Clinical trials have yielded conflicting results on immunotherapy response rates in elderly patients, partly because the precise definition of elderly varies between studies. However, several studies have reported similar response rates to ICB between elderly and middle-aged patients (33,41,55–58). For patients that do not respond to immunotherapy, it is still unknown whether the underlying mechanisms driving resistance are the same with advanced age. It is possible that a reduction in TCR diversity drives resistance to immunotherapy to a greater extent in the elderly, who are likely over-represented among cancer patients with deficient TCR repertoires. Indeed, longitudinal studies profiling immune cells in human circulation have revealed that TCR diversity significantly decreases over lifespan (12), and is also a predictive biomarker for response to immunotherapies targeting the PD-1 pathway (53,59). Our studies also indicate that TCR Vβ usage changes with advanced age in mice (20 months), resulting in decreased TCR diversity of the peripheral $CD8^+$ T-cell pool. While dynamic changes in the TCR repertoire after one cycle of anti-PD-1 treatment also correlate with therapeutic response in humans, the predictive molecular changes differ with patient age. In patients <70 years of age, increased TCR diversity is associated with favorable outcomes after a single dose of anti-PD-1 therapy, meaning that a greater number of unique TCRs are detected in the bloodstream of younger patients that control tumors with therapy (60). By contrast, increased TCR clonality is predictive for response in patients >70 years old, which means that a small number of T cells identified by unique TCR receptor sequences expand, usually by proliferation. These may represent T cells that can recognize tumor antigens, although this remains to be determined. As tumor neoantigens arise in older patients, there may not be a TCR present that recognizes the neoantigen. These studies highlight how diminished TCR diversity below a critical threshold in some elderly patients may license tumor outgrowth and limit responsiveness to ICB.

Aging is also linked to changes in T-cell differentiation states that may impact immune responses (18,32). These cells are generally characterized by markers of differentiation, including CD44, but are otherwise phenotypically heterogenous. Our study revealed expansion of $CD8^+$ T cells expressing activation and differentiation-associated markers like CD44, PD-1, and TBET in tdLNs of aged animals, consistent with system-wide inflammatory changes associated with aging. In addition, we found that adoptively transferred naïve young OT-I cells preferentially accumulated in tdLNs of aged but not young adult mice. While these results do not

rule out potential trafficking deficits within secondary lymphoid organs of aged animals, they indicate that aged tdLNs can support the activation and expansion of antigen-specific T cells.

We further demonstrated that provision of tumor-specific T-cell clones alone was not sufficient to drive durable antitumor activity in aged animals. This finding suggests that T cell–extrinsic components within the aged environment play an important role in limiting antitumor T-cell activity. While the activation state of adoptively transferred OT-I T cells was enhanced in aged versus young recipient mice at early time points, these mice failed to durably control tumor outgrowth. Likewise, anti-PD-1 therapy prolonged the survival of aged recipients of young tumor-specific $CD8^+$ T cells, but these animals still did not clear tumors as effectively as young mice. Given that exposure to an aged environment can convert young $CD8^+$ T cells into cells that resemble dysfunctional aged T cells (18), additional age-associated factors, such as cytokine levels, local microenvironment, and host metabolism may collectively contribute to deficits in antitumor immunity.

Our results highlight the importance of considering antigen specificity in studies of antitumor $CD8^+$ T-cell responses in aged animals. Experiments measuring bulk T-cell responses may disproportionately report on bystander T cells that nonspecifically expand within the highly inflammatory environment within aged hosts. In addition, our study revealed that the failure of aged mice to mobilize antitumor $CD8^+$ T cells was preceded by a reduction in tumor antigen-specific–$CD8^+$ T cells. These findings are consistent with studies in humans and mice detailing age-related attrition in TCR diversity (8,12,61–63). This feature is not unique to antitumor immunity. In fact, aged mice also exhibit a substantial reduction in numbers of antiviral precursor cells, which limit antiviral $CD8^+$ T-cell responses (20,26). Our studies similarly indicate that the loss of tumor-reactive T-cell clones in aged mice coincided with a reduction in TCR diversity. We also uncovered temporally distinct patterns of numerical and functional decline for $CD8^+$ T cells associated with antigen specificity. While OVA-reactive $CD8^+$ T cells declined in number around 8 months of age, the T cells remaining expressed effector proteins like GZMB upon tumor challenge. On the other hand, TRP-2–reactive $CD8^+$ T cells were retained for a longer time but exhibited decreased expression of effector proteins between 8-20 months of age upon tumor challenge. What drives these distinct patterns of decline is not known and is an interesting question for follow-up studies.

Immune senescence is a general term that describes age-related changes to the immune system that impair its function. Aging is a complex process and there are multiple kinds of cellular decline that occur simultaneously. Among human T cells, the loss of activating surface receptors is often used to identify cells with features of senescence (3,64). Consistent with intrinsic functional deficits, T cells isolated from aged hosts are hyporesponsive (16,17,65). Our discovery that T-cell specificity stratified effector function in an aged setting further adds to our understanding of immune senescence. Compared to strong antigens like SIINFEKL, T cells that recognize weaker antigens (TRP-2) were present at higher frequencies within tumors implanted in aged mice but lacked expression of effector proteins. SIINFEKL-reactive T cells, by contrast, were relatively rare in an aged setting but expressed protein markers linked to activation and functionality. Whether there are distinct programs of T-cell senescence linked to specificity that arise at different stages during the aging process is not known. Likewise, whether T-cell senescence contributes to the contraction of tumor antigen–

reactive T-cell clones by biasing attrition or driving clonal expansion is an interesting question that remains to be determined.

Future studies will need to consider how primary deficiencies in tumor-reactive T cells can obscure other meaningful phenotypes when using mice to model human immune aging. Here, we made use of implantable syngeneic models to study the interaction between an aged immune system and growing tumor. Our studies resolved an important conceptual gap in the aging cancer immunology literature by identifying the loss of tumor antigen–specific T cells as a fundamental barrier for the elicitation of protective antitumor immunity in aged mice. Provision of tumor-reactive T-cell clones not only induced antitumor activity in aged tumor-bearing hosts, but effectively licensed cancer immunotherapy with PD-1 inhibition. This illuminates a fundamental mechanism why aged mice are recalcitrant to therapy with ICB (35,37,41), and further explains why studies in 1-year versus 2-year old animals may come to different outcomes. These observations have important ramifications for the interpretation and design of all cancer studies that use C57BL/6J mice as a pre-clinical aging model. By assuming that tumor-antigen specificity is intact in aged hosts, age-related T-cell dysfunction may be inadvertently conflated with bystander $CD8^+$ T-cell responses. Our manuscript therefore provides a roadmap to study antigen-directed T-cell responses in the aged setting, which is a critical requirement for accurate pre-clinical modeling for cancer immunology. It will be interesting for future studies to explore how aging changes antitumor immunity in other cancer models that arise in different tissue contexts and with distinct oncogenic drivers. It is also important to note that the tumor immunology field also lacks consensus on the definition of an aged mouse. Our studies highlight how the T cells dynamically change over lifespan, meaning that the age of tumor implantation impacts core features of the T-cell response. These are all important considerations for the use of animals as pre-clinical models for the study of aging in cancer. An improved understanding of how aging reprograms T-cell immunity should contribute to rational design of cancer immunotherapies and precision medicine for the elderly.

AUTHORS' CONTRIBUTIONS

S. Han, P. Georgiev, A. E. Ringel, A. H. Sharpe & M. C. Haigis: Conceptualization, data curation, formal analysis, validation, investigation, visualization, methodology, writing-original draft, project administration, writing-review and editing, funding acquisition (**S. Han & P. Georgiev:** are equally contributing co-first authors). **A. Huang**: Resources, methodology. **T. H. Nguyen, J. M. Drijvers:** Resources, data curation, methodology, writing review and editing. **H. Creasey, J. A. Pereira, C-H. Yao, J. S. Park, T. S. Conway, D. Liang, M. Peluso:** Data curation, methodology. **M. E. Fung, S. Joshi**: Resources, data curation, methodology. **J. H. Rowe, B. C. Miller**: Resources, methodology, writing- review and editing. **G. J. Freeman**: Resources, methodology.

ACKNOWLEDGEMENTS

We would like to thank Dr. Naomi Goldman for technical assistance.

REFERENCES

1. Aunan JR, Watson MM, Hagland HR, Soreide K. Molecular and biological hallmarks of ageing. Br J Surg. 2016;103:e29--46.
2. López-Otín C, Blasco MA, Partridge L, Serrano M, Kroemer G. Hallmarks of aging: An expanding universe. Cell. Cell; 2023;186:243–78.
3. Weyand CM, Goronzy JJ. Aging of the Immune System. Mechanisms and Therapeutic Targets. Ann Am Thorac Soc. United States; 2016;13 Suppl 5:S422–8.
4. Montecino-Rodriguez E, Berent-Maoz B, Dorshkind K. Causes, consequences, and reversal of immune system aging. J Clin Invest. American Society for Clinical Investigation; 2013;123:958–65.
5. Franceschi C, Garagnani P, Parini P, Giuliani C, Santoro A. Inflammaging: a new immune–metabolic viewpoint for age-related diseases. Nat Rev Endocrinol. 2018;14:576–90.
6. Chen DS, Mellman I. Oncology meets immunology: The cancer-immunity cycle. Immunity. 2013;39:1–10.
7. Goronzy JJ, Weyand CM. Mechanisms underlying T cell ageing. Nature Reviews Immunology 2019 19:9. Nature Publishing Group; 2019;19:573–83.
8. Czesnikiewicz-Guzik M, Lee W-W, Cui D, Hiruma Y, Lamar DL, Yang Z-Z, et al. T cell subset-specific susceptibility to aging. Clinical Immunology. 2008;127:107–18.
9. Jergovic M, Smithey MJ, Nikolich-Zugich J. Intrinsic and extrinsic contributors to defective CD8+ T cell responses with aging. Exp Gerontol. 2018;105:140–5.
10. Mittelbrunn M, Kroemer G. Hallmarks of T cell aging. Nature Immunology 2021 22:6. Nature Publishing Group; 2021;22:687–98.
11. Li M, Yao D, Zeng X, Kasakovski D, Zhang Y, Chen S, et al. Age related human T cell subset evolution and senescence. Immunity & Ageing. 2019;16:24.
12. Sun X, Nguyen T, Achour A, Ko A, Cifello J, Ling C, et al. Longitudinal analysis reveals age-related changes in the T cell receptor repertoire of human T cell subsets. J Clin Invest. American Society for Clinical Investigation; 2022;132.
13. Blackman MA, Woodland DL. The narrowing of the CD8 T cell repertoire in old age. Curr Opin Immunol. England; 2011;23:537–42.
14. Goronzy JJ, Fang F, Cavanagh MM, Qi Q, Weyand CM. Naive T cell maintenance and function in human aging. J Immunol. United States; 2015;194:4073–80.
15. Ron-Harel N, Sharpe AH, Haigis MC. Mitochondrial metabolism in T cell activation and senescence: A mini-review. Gerontology. 2015;61:131–8.
16. Ron-Harel N, Notarangelo G, Ghergurovich JM, Paulo JA, Sage PT, Santos D, et al. Defective respiration and one-carbon metabolism contribute to impaired naive T cell activation in aged mice. Proc Natl Acad Sci U S A. 2018;115:13347–52.
17. Pieren DKJ, Smits NAM, van de Garde MDB, Guichelaar T. Response kinetics reveal novel features of ageing in murine T cells. Sci Rep. 2019;9:5587.
18. Mogilenko DA, Shpynov O, Andhey PS, Arthur L, Swain A, Esaulova E, et al. Comprehensive Profiling of an Aging Immune System Reveals Clonal GZMK+ CD8+ T Cells as Conserved Hallmark of Inflammaging. Immunity. Cell Press; 2021;54:99-115.e12.
19. Jiang J, Fisher EM, Murasko DM. CD8 T cell responses to influenza virus infection in aged mice. Ageing Res Rev. 2011;10:422–7.
20. Decman V, Laidlaw BJ, Doering TA, Leng J, Ertl HCJ, Goldstein DR, et al. Defective CD8 T cell responses in aged mice are due to quantitative and qualitative changes in virus-specific precursors. J Immunol. 2012;188:1933–41.

21. Decman V, Laidlaw BJ, DiMenna LJ, Abdulla S, Mozdzanowska K, Erikson J, et al. Cell-Intrinsic Defects in the Proliferative Response of Antiviral Memory CD8 T Cells in Aged Mice upon Secondary Infection. The Journal of Immunology. 2010;ji_0902063.
22. Wong C, Goldstein DR. Impact of aging on antigen presentation cell function of dendritic cells. Curr Opin Immunol. 2013;25:535–41.
23. McElhaney JE. Influenza vaccine responses in older adults. Ageing Res Rev. 2011;10:379–88.
24. Brien JD, Uhrlaub JL, Hirsch A, Wiley CA, Nikolich-Zugich J. Key role of T cell defects in age-related vulnerability to West Nile virus. J Exp Med. United States; 2009;206:2735–45.
25. Cicin-Sain L, Smyk-Pearson S, Currier N, Byrd L, Koudelka C, Robinson T, et al. Loss of naive T cells and repertoire constriction predict poor response to vaccination in old primates. J Immunol. United States; 2010;184:6739–45.
26. Yager EJ, Ahmed M, Lanzer K, Randall TD, Woodland DL, Blackman MA. Age-associated decline in T cell repertoire diversity leads to holes in the repertoire and impaired immunity to influenza virus. J Exp Med. United States; 2008;205:711–23.
27. Zhao T V, Sato Y, Goronzy JJ, Weyand CM. T-Cell Aging-Associated Phenotypes in Autoimmune Disease. Frontiers in Aging. 2022.
28. Siegel RL, Miller KD, Jemal A. Cancer statistics, 2015. CA Cancer J Clin. 2015;65:5–29.
29. Siegel RL, Miller KD, Jemal A. Cancer statistics, 2019. CA Cancer J Clin. 2019;
30. The importance of aging in cancer research. Nat Aging. 2022;2:365–6.
31. Drijvers JM, Sharpe AH, Haigis MC. The effects of age and systemic metabolism on anti-tumor T cell responses. Elife. England; 2020;9.
32. Han S, Georgiev P, Ringel AE, Sharpe AH, Haigis MC. Age-associated remodeling of T cell immunity and metabolism. Cell Metab. 2023;31:36–55.
33. Sceneay J, Goreczny GJ, Wilson K, Morrow S, DeCristo MJ, Ubellacker JM, et al. Interferon Signaling Is Diminished with Age and Is Associated with Immune Checkpoint Blockade Efficacy in Triple-Negative Breast Cancer. Cancer Discov. United States; 2019;9:1208–27.
34. Sekido K, Tomihara K, Tachinami H, Heshiki W, Sakurai K, Moniruzzaman R, et al. Alterations in composition of immune cells and impairment of anti-tumor immune response in aged oral cancer-bearing mice. Oral Oncol. 2019;99:104462.
35. Garcia MG, Deng Y, Murray C, Reyes RM, Padron A, Bai H, et al. Immune checkpoint expression and relationships to anti-PD-L1 immune checkpoint blockade cancer immunotherapy efficacy in aged versus young mice. Aging Cancer. United States; 2022;3:68–83.
36. Lin P-Y, Sun L, Thibodeaux SR, Ludwig SM, Vadlamudi RK, Hurez VJ, et al. B7-H1-dependent sex-related differences in tumor immunity and immunotherapy responses. J Immunol. United States; 2010;185:2747–53.
37. Padrón Á, Hurez V, Gupta HB, Clark CA, Pandeswara SL, Yuan B, et al. Age effects of distinct immune checkpoint blockade treatments in a mouse melanoma model. Exp Gerontol. England; 2018;105:146–54.
38. Oh J, Magnuson A, Benoist C, Pittet MJ, Weissleder R. Age-related tumor growth in mice is related to integrin α4 in CD8+ T cells. JCI Insight. American Society for Clinical Investigation; 2018;3:e122961.
39. Mirza N, Duque MA, Dominguez AL, Schrum AG, Dong H, Lustgarten J. B7-H1 Expression on Old CD8+ T Cells Negatively Regulates the Activation of Immune Responses in Aged Animals. The Journal of Immunology. American Association of Immunologists; 2010;184:5466–74.

40. Kugel CH 3rd, Douglass SM, Webster MR, Kaur A, Liu Q, Yin X, et al. Age Correlates with Response to Anti-PD1, Reflecting Age-Related Differences in Intratumoral Effector and Regulatory T-Cell Populations. Clin Cancer Res. United States; 2018;24:5347–56.
41. Nakajima Y, Chamoto K, Oura T, Honjo T. Critical role of the CD44(low)CD62L(low) CD8(+) T cell subset in restoring antitumor immunity in aged mice. Proc Natl Acad Sci U S A. United States: National Academy of Sciences; 2021;118.
42. Hogquist KA, Jameson SC, Heath WR, Howard JL, Bevan MJ, Carbone FR. T cell receptor antagonist peptides induce positive selection. Cell. 1994;76:17–27.
43. Stuart T, Butler A, Hoffman P, Hafemeister C, Papalexi E, Mauck WM 3rd, et al. Comprehensive Integration of Single-Cell Data. Cell. 2019;177:1888--1902.e21.
44. Hafemeister C, Satija R. Normalization and variance stabilization of single-cell RNA-seq data using regularized negative binomial regression. Genome Biol. 2019;20:296.
45. Zeng J, Zhang Y, Shang Y, Mai J, Shi S, Lu M, et al. CancerSCEM: a database of single-cell expression map across various human cancers. Nucleic Acids Res. England; 2022;50:D1147–55.
46. Bindea G, Mlecnik B, Tosolini M, Kirilovsky A, Waldner M, Obenauf AC, et al. Spatiotemporal dynamics of intratumoral immune cells reveal the immune landscape in human cancer. Immunity. United States; 2013;39:782–95.
47. Ringel AE, Drijvers JM, Baker GJ, Catozzi A, García-Cañaveras JC, Gassaway BM, et al. Obesity Shapes Metabolism in the Tumor Microenvironment to Suppress Anti-Tumor Immunity. Cell. 2020;183:1848--1866.e26.
48. Liu J, Lichtenberg T, Hoadley KA, Poisson LM, Lazar AJ, Cherniack AD, et al. An Integrated TCGA Pan-Cancer Clinical Data Resource to Drive High-Quality Survival Outcome Analytics. Cell. United States; 2018;173:400-416.e11.
49. Flurkey K, Currer JM, Harrison DE. Mouse Models in Aging Research. The Mouse in Biomedical Research. Academic Press; 2007;3:637–72.
50. Sullivan BM, Juedes A, Szabo SJ, Von Herrath M, Glimcher LH. Antigen-driven effector CD8 T cell function regulated by T-bet. Proc Natl Acad Sci U S A. Proc Natl Acad Sci U S A; 2003;100:15818–23.
51. Intlekofer AM, Takemoto N, Wherry EJ, Longworth SA, Northrup JT, Palanivel VR, et al. Effector and memory CD8+ T cell fate coupled by T-bet and eomesodermin. Nature Immunology 2005 6:12. Nature Publishing Group; 2005;6:1236–44.
52. Hodi FS. Well-Defined Melanoma Antigens as Progression Markers for Melanoma: Insights into Differential Expression and Host Response Based on Stage. Clinical Cancer Research. American Association for Cancer Research; 2006;12:673–8.
53. Valpione S, Mundra PA, Galvani E, Campana LG, Lorigan P, De Rosa F, et al. The T cell receptor repertoire of tumor infiltrating T cells is predictive and prognostic for cancer survival. Nat Commun. England; 2021;12:4098.
54. Erbe R, Wang Z, Wu S, Xiu J, Zaidi N, La J, et al. Evaluating the impact of age on immune checkpoint therapy biomarkers. Cell Rep. United States; 2021;36:109599.
55. Kim CM, Lee JB, Shin SJ, Ahn JB, Lee M, Kim HS. The efficacy of immune checkpoint inhibitors in elderly patients: a meta-analysis and meta-regression. ESMO Open. England; 2022;7:100577.
56. Choucair K, Naqash AR, Nebhan CA, Nipp R, Johnson DB, Saeed A. Immune Checkpoint Inhibitors: The Unexplored Landscape of Geriatric Oncology. Oncologist. England; 2022;27:778–89.
57. Landre T, Des Guetz G, Chouahnia K, Fossey-Diaz V, Culine S. Immune Checkpoint Inhibitors for Patients Aged ≥ 75 Years with Advanced Cancer in First- and Second-Line Settings: A Meta-Analysis. Drugs Aging. New Zealand; 2020;37:747–54.
58. Nebhan CA, Cortellini A, Ma W, Ganta T, Song H, Ye F, et al. Clinical Outcomes and Toxic Effects of Single-Agent Immune Checkpoint Inhibitors Among Patients Aged 80

Years or Older With Cancer: A Multicenter International Cohort Study. JAMA Oncol. United States; 2021;7:1856–61.
59. Han J, Duan J, Bai H, Wang Y, Wan R, Wang X, et al. TCR Repertoire Diversity of Peripheral PD-1(+)CD8(+) T Cells Predicts Clinical Outcomes after Immunotherapy in Patients with Non-Small Cell Lung Cancer. Cancer Immunol Res. United States; 2020;8:146–54.
60. Salih Z, Banyard A, Tweedy J, Galvani E, Middlehurst P, Mills S, et al. T cell immune awakening in response to immunotherapy is age-dependent. Eur J Cancer. Elsevier Ltd; 2022;162:11–21.
61. Goronzy JJ, Lee W-W, Weyand CM. Aging and T-cell diversity. Exp Gerontol. England; 2007;42:400–6.
62. Qi Q, Liu Y, Cheng Y, Glanville J, Zhang D, Lee JY, et al. Diversity and clonal selection in the human T-cell repertoire. Proc Natl Acad Sci U S A. National Academy of Sciences; 2014;111:13139–44.
63. Rudd BD, Venturi V, Li G, Samadder P, Ertelt JM, Way SS, et al. Nonrandom attrition of the naive CD8 + T-cell pool with aging governed by T-cell receptor: pMHC interactions. Proc Natl Acad Sci U S A. National Academy of Sciences; 2011;108:13694–9.
64. Weng N-P, Akbar AN, Goronzy J. CD28(-) T cells: their role in the age-associated decline of immune function. Trends Immunol. England; 2009;30:306–12.
65. Serra JA, Fernandez-Gutierrez B, Fernandez-Garcia C, Vidan M, Banares A, Ribera JM, et al. Early T Cell Activation in Elderly Humans. Age Ageing. 1996;25:470–8.

Figure Legends

Figure 1. Immunogenic tumors grow more rapidly in aged versus young mice.
(**A**) Tumor growth curves in young (2-4 month) versus aged (20-24 month) wild-type C57BL/6J mice inoculated with $2.5x10^5$ MC38 colorectal cancer (young, n = 17; aged, n = 13), $2.5x10^5$ EO771 breast cancer (young, n = 20; aged, n = 17), or $2.5x10^5$ B16 melanoma cells (n = 6 per group). Graphs depict mean tumor size.
(**B-C**) Tumor growth curves (**B**) and survivorship (**C**) of young (2-4 month) versus aged (20-24 month) wild-type C57BL/6J mice inoculated with OVA-expressing MC38, EO771, or B16 cancer cells ($2.5x10^5$ cell per mouse; n = 10 per group).
(**D-E**) Tumor growth curves following implantation of MC38 colorectal (**D**) or EO771 breast (**E**) tumor cells in young versus aged wild-type C57BL/6J mice treated with isotype control or anti-CD8 depleting antibodies (n = 8 per group).

Statistics: Results are representative of at least 2 independent experiments per tumor model. Graphs depict mean ± standard error of the mean (SEM). Statistical comparisons between conditions were performed by two-way ANOVA with Bonferroni test to correct for multiple comparisons (**A-B**, **D**). Survival statistics were performed by log-rank test (**C**). P-values: *p ≤ 0.05, **p ≤ 0.01, ***p ≤ 0.001, ****p ≤ 0.0001.

Figure 2. Aging reduces the functionality of tumor-infiltrating $CD8^+$ T cells.
(**A-F**) Flow cytometry analysis of immune cells in tdLN and MC38-OVA, B16-OVA and EO771-OVA tumors from young (2-4 month) versus aged (20-24 month) wild-type C57BL/6J mice on day 12 after tumor implantation [(B16-OVA young, n = 10; aged, n = 9), (MC38-OVA young, n = 8; aged, n = 6), (EO771-OVA young, n = 8; aged, n = 8)]. Quantification of the percentage of CD44 and PD-1 double positive cells among $CD8^+$ intratumoral and tdLN T cells (**A**). Quantification of the proportions of $CD8^+$ T cells with features of progenitor and more differentiated exhausted states ($Tim\text{-}3^+/TCF1^-/CD8^+/CD44^+/PD\text{-}1^+$) $CD8^+$ intratumoral and tdLN T cells (**B**). Quantification of the percentage of $CD44^+CD62L^-$ effector memory $CD8^+$ intratumoral and tdLN T cells (**C**). Quantification of T-BET expression among intratumoral and tdLN $CD8^+$ T cells (**D**). Quantification of GZMB expression among intratumoral and tdLN $CD8^+$ T cells (**E**). Quantification of MKI-67 expression among intratumoral and tdLN $CD8^+$ T cells (**F**).

Statistics: Results are representative of at least 2 independent experiments per tumor model. Each dot represents an individual animal. Statistical significance was assessed by Student's t-test (**A-F**). Graphs display mean ± standard deviation (**A-F**). P-values: *p ≤ 0.05, **p ≤ 0.01, ***p ≤ 0.001, ****p ≤ 0.0001.

Figure 3. Single-cell analysis reveals deficit in activated $CD8^+$ T-cell states in tumors within aged animals.
(**A**) Schematic depicting single-cell RNA-seq experiment and analysis.
(**B**) Identification of tumor-infiltrating $CD8^+$ T cell populations. Uniform Manifold Approximation and Projection (UMAP) embeddings of single-cell RNA-seq profiles from 8,081 $CD8^+$ T cells isolated from MC38 tumors implanted in young mice and 3,553 $CD8^+$ T cells isolated from tumors implanted in aged mice, showing seven clusters, and colored by cluster. Representative of one experiment, n = 8 young mice and n = 7 aged mice, with each mouse barcoded using TotalSeqB hashing antibodies.
(**C**) Galaxy plot depicting differences in cluster frequency by age.

(**D**) Bar plot depicting proportional differences in $CD8^+$ T cell clusters from aged versus young tumors.
(**E**) Bar plot depicting the number of differentially expressed (DE) genes per cluster (*upper*). Heatmap representing stimulation or quiescence gene score per cluster (*lower*).
(**F-I**) Trajectory analysis by Monocle2. Plot containing all cells colored by cluster (**F**). Placement of young (**G**) or aged (H) $CD8^+$ T cells along the combined trajectory. Location of cells with gene expression profiles consistent with more stimulated (red) versus more quiescent (blue) cell states along the pseudotime trajectory (**I**). Colors in F-H indicate cluster identities as in (B).

Statistics: Statistical significance was assessed by unpaired t-test (**D**) and significantly differentially expressed genes were identified by non-parametric Wilcoxon rank sum test (**E**). P-values: *p ≤ 0.05, **p ≤ 0.01, ***p ≤ 0.001.

Figure 4. Aging reduces the proportions and numbers of tumor antigen–specific cytotoxic $CD8^+$ T cells.
(**A-C**) Representative flow cytometry contour plots depicting staining of intratumoral OVA-specific $CD8^+$ T cells from young or aged mice in the MC38-OVA (**A**), B16-OVA (**B**) and EO771-OVA (**C**) tumor models at day 12 after tumor cell implantation.
(**D-E**) Quantification of the percentage (**D**) [(B16-OVA young, n = 15; aged, n = 15), (MC38-OVA young, n = 15; aged, n = 10), (EO771-OVA young, n = 15; aged, n = 14) and absolute numbers (**E**) [(B16-OVA young, n = 15; aged, n = 14), (MC38-OVA young, n = 15; aged, n = 10), (EO771-OVA young, n = 15; aged, n = 14)] of intratumoral SIINFEKL-reactive $CD8^+$ T cells from young or aged mice in the MC38-OVA, B16-OVA and EO771-OVA tumor models at day 12.
(**F-G**) Quantification of the percentage (**F**) and absolute numbers (**G**) of melanoma tumor-associated antigen-specific $CD8^+$ T cells including MuLV p15E, gp100 and TRP-2 peptide-specific T cells from young or aged mice bearing B16-OVA tumors at day 12 after tumor cell implantation (young, n = 16; aged n = 16).

Statistics: Results are representative of at least 2 independent experiments per tumor model **(A-C).** Statistical significance was assessed by Student's t-test (**D-G**). Results represent a pool of 2 independent experiments (**D-G**) . Each dot represents an individual animal. Graphs display mean ± standard deviation (**D-G**). P-values: *p ≤ 0.05, **p ≤ 0.01, ***p ≤ 0.001, ****p ≤ 0.0001.

Figure 5. TCR Vβ usage changes late in mouse lifespan.
(**A**-**D**) Dotplots depicting coefficient of variation (CV) for TCR Vβ usage among naïve $CD8^+$ T cells in different age brackets that reside in thymus (**A**), spleen (**B**), tumor-draining lymph node (tdLN) (**C**), and tumor bed of B16-OVA tumors 12 days post-implantation (**D**). Each dot represents the CV for a single Vβ gene segment among C57BL/6J animals that are 2 months (n = 18), 8 months (n = 18), 12 months (n = 18), 16 months (n = 16), and 20 months (n = 15) of age.
(**E**-**G**) Shannon diversity index calculated based on TCR Vβ usage among naïve $CD8^+$ T cells as in A-D that reside in in thymus (**E**), spleen (**F**), tumor-draining lymph node (tdLN) (**G**), and tumor bed of B16-OVA tumors (**H**).
(**I**-**L**) Dotplots depicting proportions of SIINFEKL-reactive (**I**) or TRP-2-reactive (**J**) $CD8^+$ T cells in the tumor-draining lymph node from mice bearing B16-OVA tumors. Dotplots depicting proportions of SIINFEKL-reactive (**K**) or TRP-2-reactive (**L**) $CD8^+$ T cells in the tumor bed of B16-OVA tumors on day 12 post-implantation.
(**M**-**N**) Dotplots depicting Granzyme B expression in SIINFEKL-reactive (**M**) or TRP-2-reactive (**N**) $CD8^+$ T cells isolated from B16-OVA tumors on day 12 post-implantation.

(**O**-**P**) Dotplots depicting the frequencies of PD-1$^+$ TIM3$^+$ CD8$^+$ SIINFEKL-reactive (**O**) or TRP-2-reactive (**P**) CD8$^+$ T cells isolated from B16-OVA tumors on day 12 post-implantation.

Statistics: Results are pooled from 2 independent experiments. Each dot represents an individual animal. Significance assessed by one-way analysis of variance (ANOVA) with Tukey's correction for multiple hypothesis testing (**A**-**N**). Each dot represents an individual animal. Graphs display mean ± standard deviation. P-values: *p ≤ 0.05, **p ≤ 0.01, ***p ≤ 0.001, ****p ≤ 0.0001.

Figure 6. Restoring tumor-specific T cells enhances tumor control and overcomes resistance to PD-1 blockade.
(**A**) Experimental schematic. PBS control or 10,000 naïve young (2-4 month) OT-I CD8$^+$ T cells were adoptively transferred into young (2-4 months) or aged (20-24 months) recipients one day before tumor implantation (day -1). B16-OVA or MC38-OVA cells (2.5x10^5 cells) were injected subcutaneously in young and aged mice on day 0.
(**B**) B16-OVA tumor growth in young (2-4 month) versus aged (20-24 month) wild-type C57BL/6J mice injected with mock PBS or young (2-4 month) OT-I CD8$^+$ T cells (young, n = 10; young + young OT-1, n = 8; aged, n = 8; aged + young OT-1, n = 8).
(**C**) Percent Tumor growth inhibition (TGI) following adoptive transfer of young (2-4 month) OT-I T cells in B16-OVA tumor-bearing young or aged mice was quantified using the following formula: % TGI = [(Tumor vol. of control – Tumor vol. of OT-I treated) / (Tumor vol. of control)] x 100.
(**D**) Survivorship of tumor-bearing young versus aged mice injected with PBS or young (2-4 month) OT-I CD8$^+$ T cells.
(**E-J**) OT-I CD8$^+$ T cell proportion and phenotypes in B16-OVA and MC38-OVA tumor-bearing young or aged mice. % OT-I T cells amongst total CD8$^+$ T cells were quantified in tdLN and tumor of B16-OVA (**E**) or MC38-OVA (**F**) tumor-bearing mice [(B16-OVA young, n = 8; aged, n = 8), (MC38-OVA young, n = 5; aged =7)]. %MKI-67$^+$, PD-1$^+$ and T-BET$^+$ OT-I CD8$^+$ T cells in tdLN (**G, H**) and tumor (**I, J**) of B16-OVA (**G, I**) and MC38-OVA (**H, J**) tumor-bearing.
(**K**) Tumor growth curves (n = 10 per group) and survivorship (n = 18 per group) of B16-OVA tumor-bearing young (2-4 month) versus aged (20-24 month) wild-type C57BL/6J mice injected with isotype control or anti-PD-1 (29F.1A12).
(**L**) Experimental schematic of the combined OT-I T cell transfers and PD-1 blockade in young vs. aged mice.
(**M-N**) Tumor growth curves (n = 8 per group) and survival (n = 16 per group) of B16-OVA melanoma-bearing young (2-4 month) (**M**) versus aged (20-24 month) (**N**) wild-type C57BL/6J mice injected with OT-I CD8$^+$ T cells and/or anti-PD-1.

Statistics: Results are representative of at least 2 independent experiments per tumor model. Statistical significance was assessed by Student's t-test (**E-J**) and tumor growth curves depict mean ± SEM (**B, K, M-N**). Survival statistics were performed by log-rank test. P-values: *p ≤ 0.05, **p ≤ 0.01, ***p ≤ 0.001 and ****p ≤ 0.0001.

Figure 7. CD8$^+$ T cell–associated immune deficits in human patient tumors during aging.
(**A**) Boxplot depicting CD8$^+$ T cell infiltration scores calculated based on gene expression data from patient tumors (n = 9,286) across all tumor types in The Cancer Genome Atlas (TCGA), separated by diagnosis age.
(**B-C**) Bioinformatics analysis of single cell RNA-sequencing datasets from the Cancer Single-cell Expression Map (CancerSCEM) database of tumor-infiltrating immune cells in human

patients. Volcano plot depicting significant correlations between total immune cell frequencies (**B**) or lymphocyte subset frequencies (**C**) and patient age. Tcm is an abbreviation for "Central Memory T cells". Red dots depict immune populations where cell frequency is significantly positively associated with age across tumor samples. Blue dots depict immune populations where cell frequency is significantly negatively associated with age across tumor samples.
(**D**) Scatterplot depicting the significant negative correlation between the proportion of $CD8^+$ Effector T cells as a fraction of total $CD8^+$ T cells in tumors with patient age.
(**E-G**) Survival analysis of patient data from The Cancer Genome Atlas (TCGA). Progression-free interval in days for young (**E**) or aged (**F**) cancer patients grouped by median T cell score. Bar plots depicting the percent difference in median Progression-Free Interval (PFI) between patients that score in the top or bottom 50^{th} percentile for immune gene signatures, comparing young versus aged patient groups (**G**), calculated as $100*(\text{median } PFI_{Aged,\ High} - \text{median } PFI_{Aged,\ Low})/(\text{median } PFI_{Aged,\ Total})$ or $100*(\text{median } PFI_{Young,\ High} - \text{median } PFI_{Young,\ Low})/(\text{median } PFI_{Young,\ Total})$.

Statistics: Significance assessed by Kruskal-Wallis one-way analysis of variance (**A**). Correlation coefficients are calculated as Spearman's rank correlation coefficient (**B-D**). Significant correlations are calculated as asymptotic P-values (**B-D**). Between-group significance in survival analysis assessed using a log-rank test (**E-G**).

Figure 1

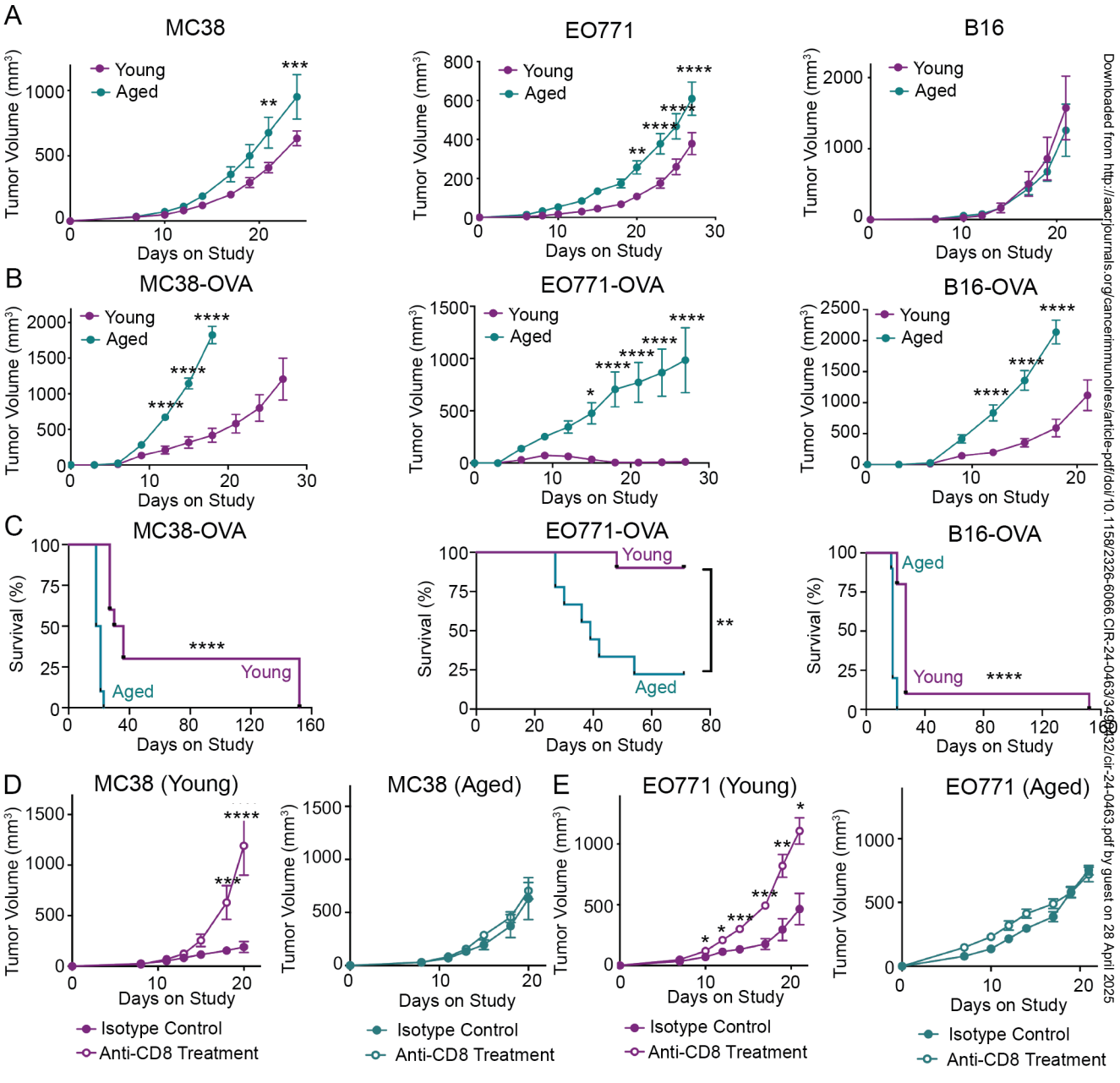

Figure 2

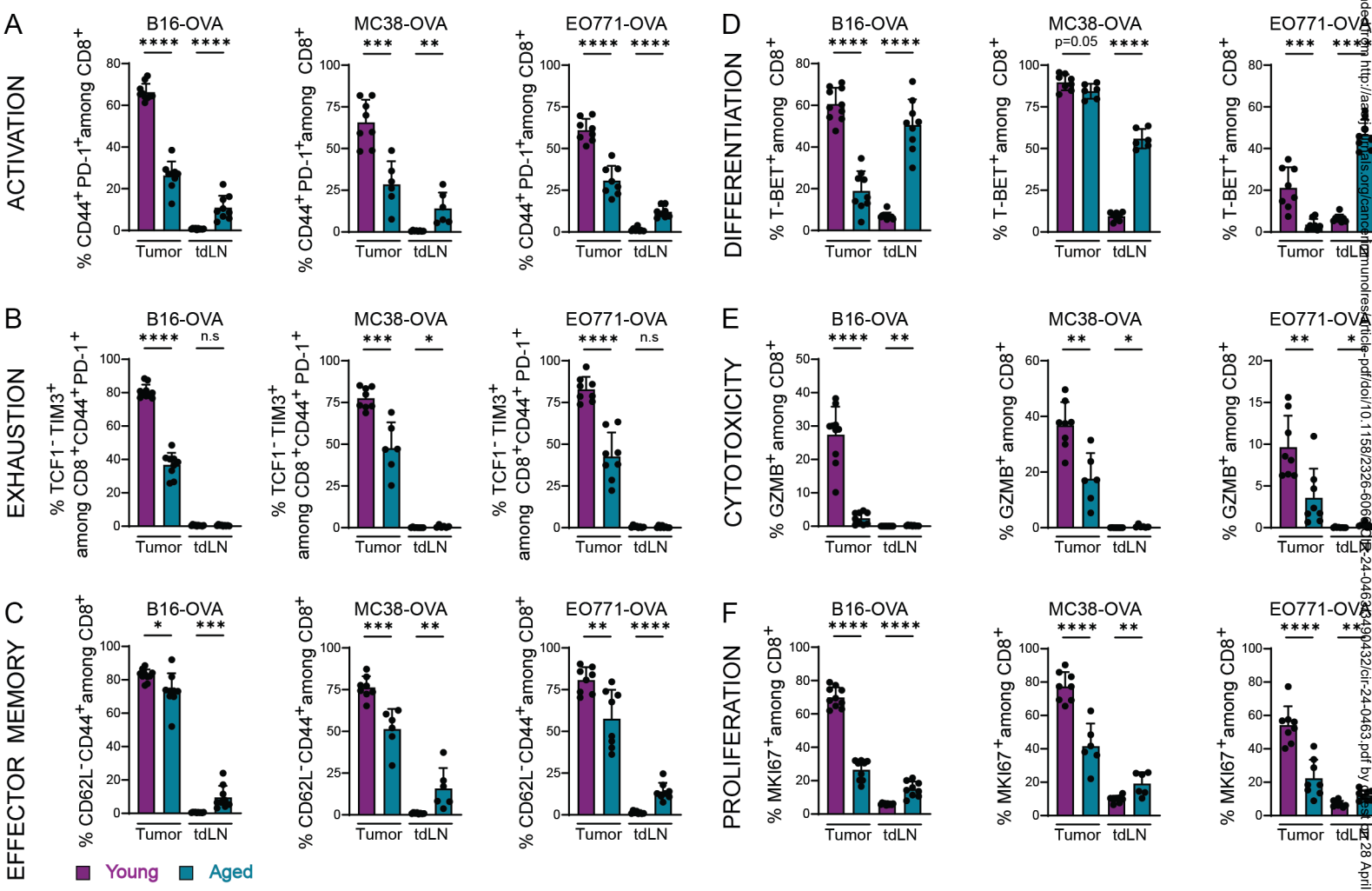

Figure 3

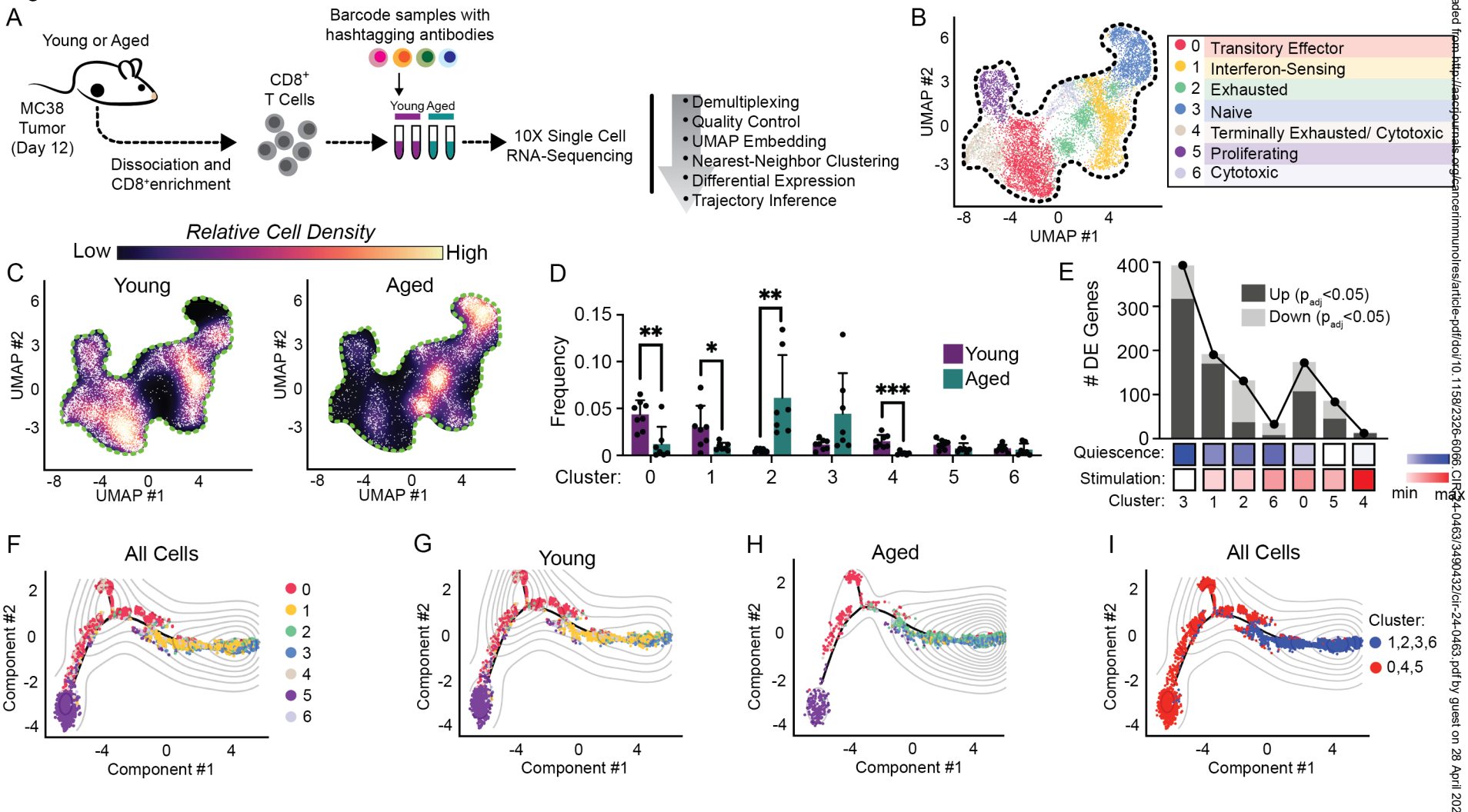

Figure 4

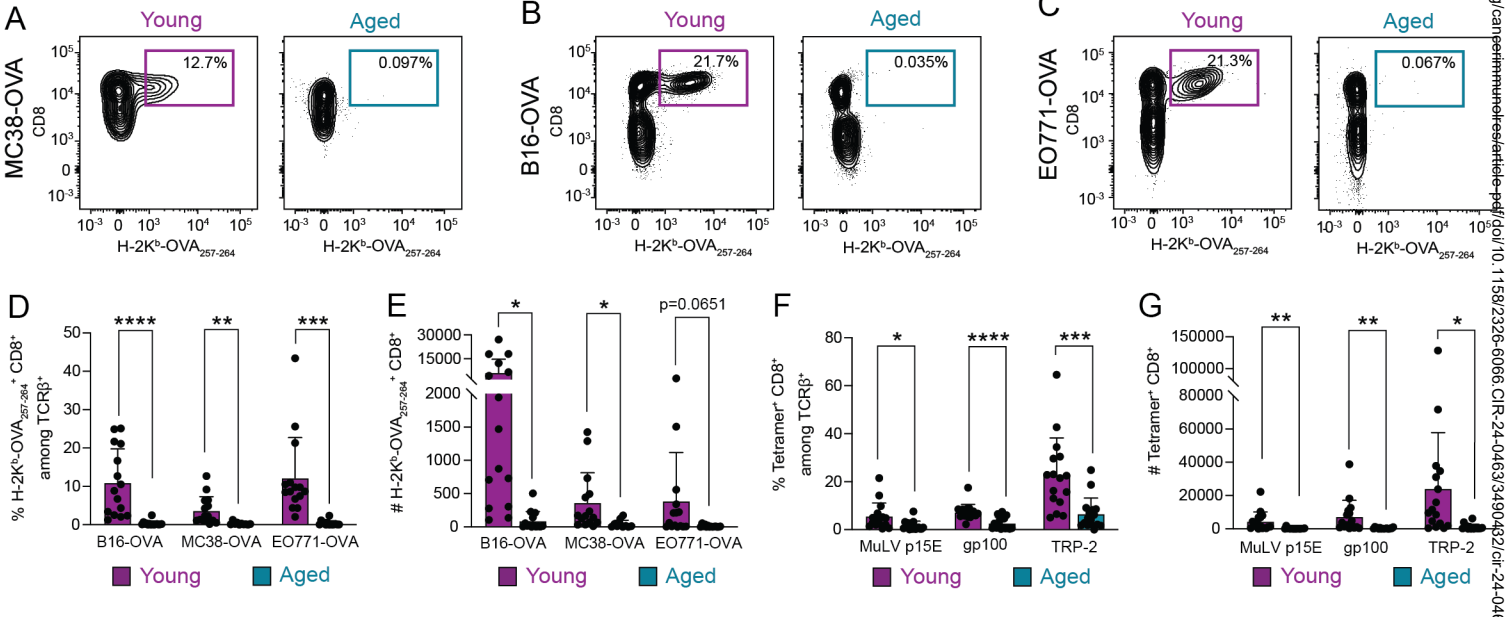

Figure 5

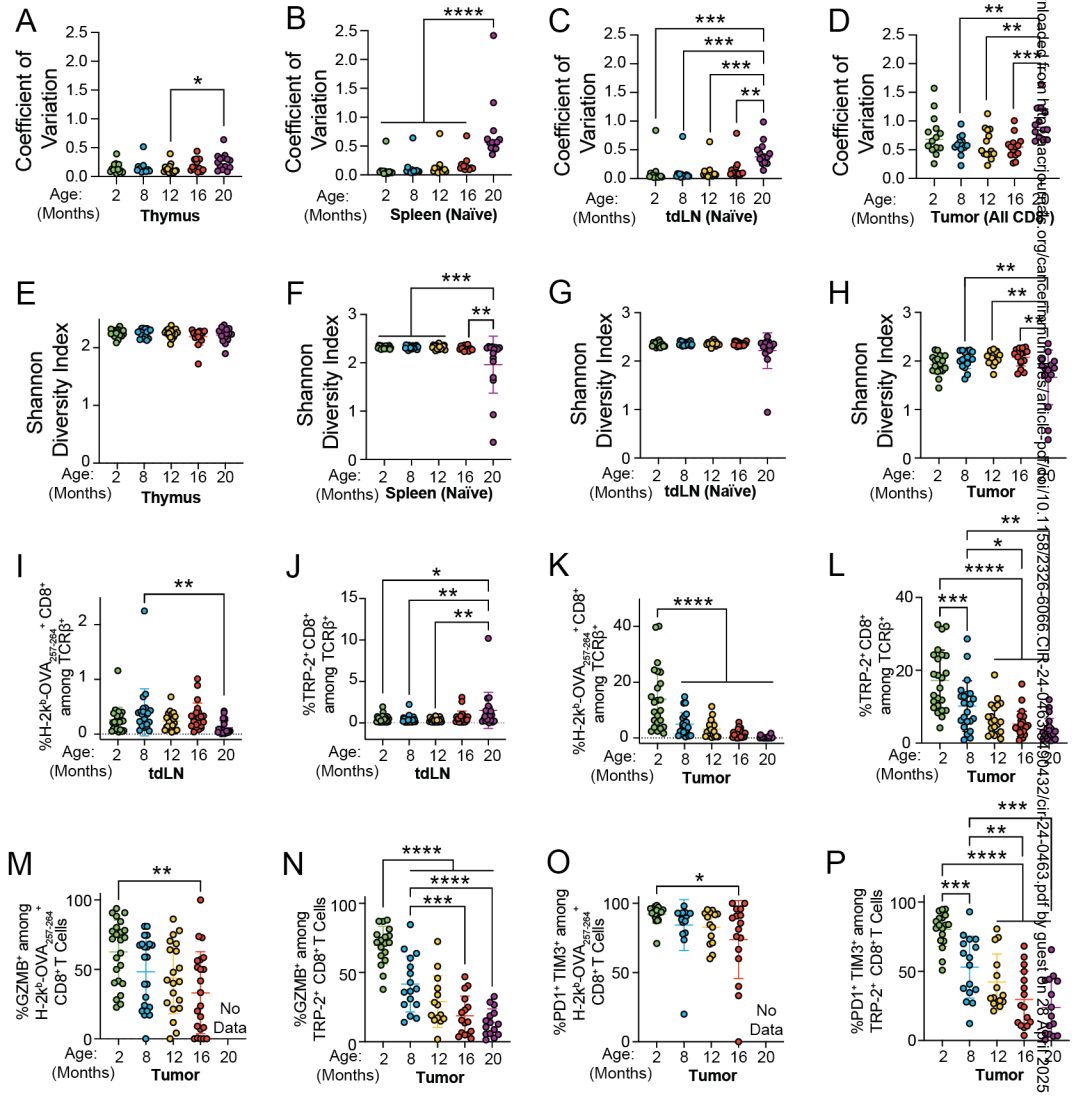

Figure 6

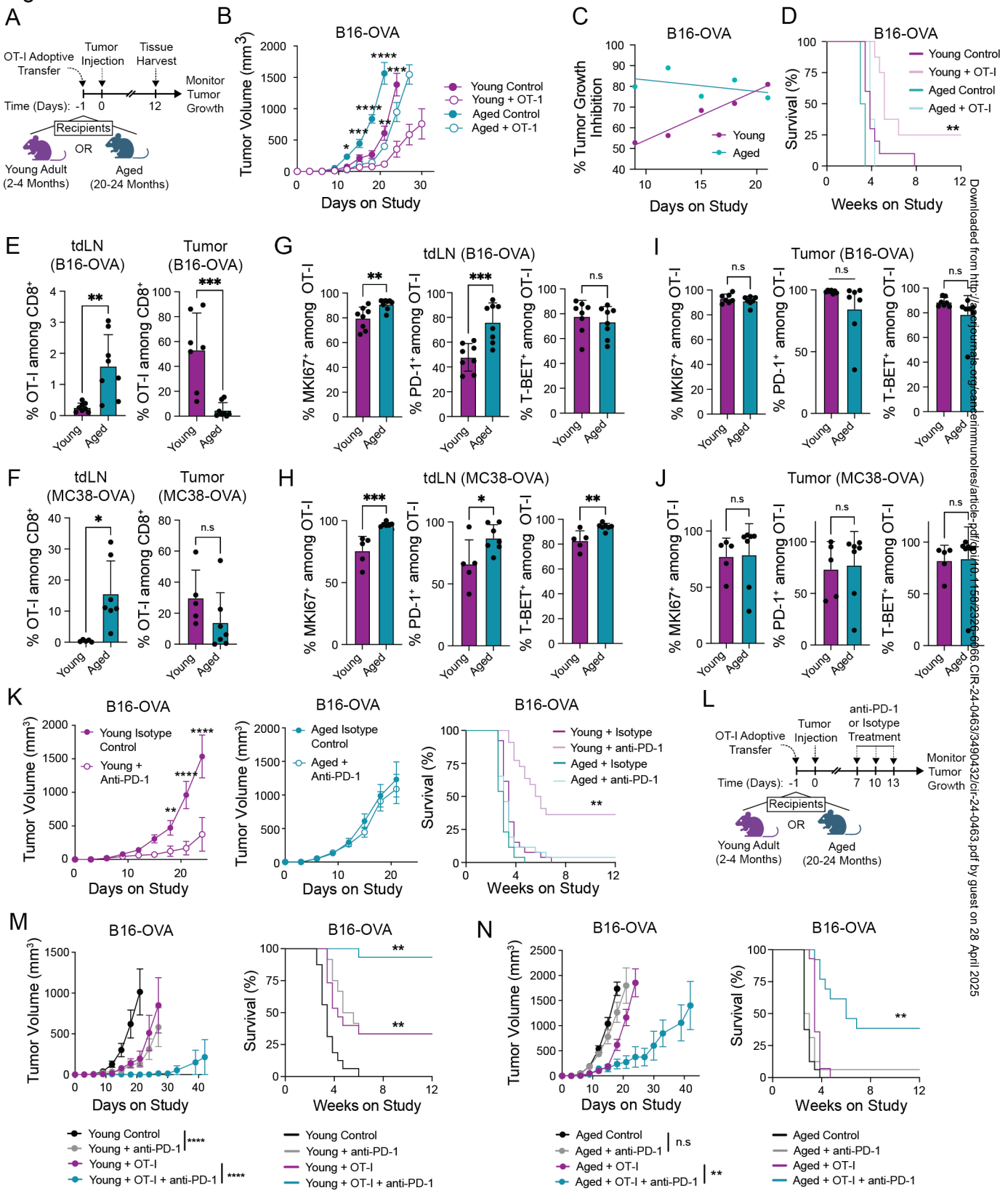

Figure 7